

**INVESTIGATION OF COLLISION PROBABILITY
OF ELECTRONS AND IONS WITH
ALKALI METAL ATOMS**

PREPARED BY R. H. BULLIS AND W. L. NIGHAN

**SEMIANNUAL REPORT
NOVEMBER 1964**

PREPARED UNDER CONTRACT NO. NAS3-4171

GPO PRICE \$
OTS PRICE(S) \$
Hard copy (HC) \$ 3.00
Microfiche (MF) \$ 1.75

N 65 12017

(ACCESSION NUMBER)

63
(PAGES)

CR-54223
(NASA CR OR TMX OR AD NUMBER)

(THRU)

1
(CODE)

25
(CATEGORY)

FACILITY FORM 602

BY

United Aircraft Research Laboratories

**U
A**

UNITED AIRCRAFT CORPORATION

EAST HARTFORD, CONNECTICUT

FOR

**NATIONAL AERONAUTICS & SPACE ADMINISTRATION
LEWIS RESEARCH CENTER
CLEVELAND, OHIO**

NOTICE

This report was prepared as an account of Government-sponsored work. Neither the United States nor the National Aeronautics and Space Administration (NASA), nor any person acting on behalf of NASA:

- A) Makes any warranty or representation, expressed or implied, with respect to the accuracy, completeness, or usefulness of the information contained in this report, or that the use of any information, apparatus, method, or process disclosed in this report may not infringe privately-owned rights; or
- B) Assumes any liabilities with respect to the use of, or for damages resulting from the use of any information, apparatus, method or process disclosed in this report.

As used above, "person acting on behalf of NASA" includes any employee or contractor of NASA, or employee of such contractor, to the extent that such employee or contractor of NASA or employee of such contractor prepares, disseminates, or provides access to, any information pursuant to his employment or contract with NASA, or his employment with such contractors.

Requests for copies of this report should be referred to

National Aeronautics and Space Administration
Office of Scientific and Technical Information
Washington 25, D.C.
Attention: AFSS-A

CASE FILE COPY

29743

UNITED AIRCRAFT CORPORATION
RESEARCH LABORATORIES
East Hartford, Connecticut

NASA Report No.: CR-54223

United Aircraft Corporation Research Laboratories Report No.: C-920243-6
Semiannual Report

Date of Reporting Period: April 22, 1964, to October 21, 1964

Title of Contract: Investigation of Collision Probability of Electrons and
Ions with Alkali Metal Atoms

Contract Number: NAS3-4171

Contractor: United Aircraft Corporation Research Laboratories
East Hartford, Connecticut

203-528-4811

Principal Investigator: R. H. Bullis

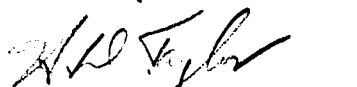
National Aeronautics & Space Administration
Lewis Research Center
Space Power Systems Division
Project Manager: Mr. H. E. Nastelin, MS 500-309

Reported By:


R. H. Bullis


W. L. Nighan

Approved By:


H. D. Taylor, Manager
Physics Department

Date: November 10, 1964

Report C-920243-6

Semiannual Report Under Contract NAS3-4171
for the Period April 22, 1964, through October 21, 1964

Investigation of Collision Probability of Electrons and Ions
with Alkali Metal Atoms

TABLE OF CONTENTS

	Page
SUMMARY	1
CESIUM ION-ATOM TOTAL COLLISION PROBABILITY MEASUREMENTS	2
Introduction	2
Description of the Experiment	3
Measurements and Results	6
Outline of Research for the Next Six-Month Period	9
ELECTRON CESIUM-ATOM COLLISION PROBABILITY MEASUREMENTS	10
Introduction	10
Theory and Plasma Model	10
Description of the Experiment	13
Measurements and Results	14
Analysis of Trial Functions for the Cross Section	17
Outline of Research for the Next Six-Month Period	20
REFERENCES	21-22
LIST OF FIGURES	23
FIGURES	23-A
APPENDIX I	I-1 - 12
APPENDIX II	II-1
DISTRIBUTION LIST	III-1 - 8

Report C-920243-6

Investigation of Collision Probability of Electrons and

Ions with Alkali Metal Atoms

Semiannual Progress Report - April 22, 1964, to October 21, 1964

Contract NAS3-4171

Summary

12017

This report is a summary of the experimental research investigations conducted at the United Aircraft Corporation Research Laboratories to determine the collision probabilities of electrons and cesium ions with cesium atoms during the first six-month period from April 22, 1964, to October 21, 1964, under contract NAS3-4171. In previous studies under Contract NASr-112, electron cyclotron resonance techniques were employed to measure the electron-cesium atom collision probability over an energy range from 0.05 to 0.10 eV. A modified Ramsauer beam experiment was employed under the same contract to measure the collision probability of cesium ions with cesium atoms over the energy range from 0.12 to 9.7 eV. The results of these investigations were reported at the IEEE Thermionic Converter Specialist Conference, Gatlinburg, Tennessee, on October 7 to 9, 1963. The work under this present contract represents an extension of these earlier investigations. A cesium arc discharge is being used in conjunction with electrostatic and rf conductivity probe techniques to determine the collision probability of electrons with cesium atoms over the energy range from 0.1 to 0.5 eV. Further cesium ion-cesium atom collision probability measurements are being made in the existing modified Ramsauer beam experiment to extend the energy range of these measurements below 0.1 eV. A knowledge of both the collision probability of electrons and cesium ions with cesium atoms is essential in the analysis of the neutralization plasma existing in the thermionic converter as well as being of importance in the analysis of other devices which employ cesium vapor in an ionized state.

Author

CESIUM ION-ATOM TOTAL COLLISION PROBABILITY MEASUREMENTS

Introduction

In order to obtain an insight into the mechanism responsible for the production of the non-equilibrium ionization which exists in the neutralization plasma of arc-mode thermionic converters, the loss rate of ions from the plasma must be accurately known. In diffusion dominated plasmas, the loss rate of ions is determined by their mobility. Preliminary measurements of the total collision cross section of cesium ions interacting with cesium atoms have been made over the energy range of 0.12 to 9.7 eV using a modified Ramsauer experiment under Contract NASr-112. The present investigations are extensions of this work to energies below 0.12 eV which is the energy range of most interest in the analysis of the neutralization plasma that exists in the converter. Knowledge of the cesium ion mobility provides an insight not only into the loss rate of ions from the plasma but also of the possible energy transfer mechanisms from the plasma to the emitter surface which can cause a significant change in the emitter surface work function.

Extrapolations of high-energy charge exchange information reported in the literature to the energy range of interest in the converter have been made by Sheldon.¹ These extrapolations, which have included approximations to account for polarization effects at energies below 1.0 eV, vary by as much as an order of magnitude. The lowest energy at which charge exchange cross sections have been measured using beam techniques is 6.0 eV (Ref. 2). Due to the nature of the experimental apparatus employed in these charge exchange measurements, no correction for contact potential effects could be made in these investigations. Therefore, the reported charge exchange cross-section information at an energy of 6.0 eV can be in serious error due to a large uncertainty in the determination of the energy of the ion beam. Other attempts have been made to determine cesium ion mobilities by observing the decay rate of the afterglow of a cesium plasma.^{3,4} In these measurements no attempt was made to determine the nature of the ion energy distribution and in some cases, the dominant ionic species existing in the plasma was not identified. In the present experiment, which uses a modified Ramsauer beam technique, contact potential effects have been eliminated from the measurement by employing an electroformed collision chamber. The energy, as well as the species of the ion beam interacting with the cesium atoms in the collision chamber, has been positively identified by mass spectrometric techniques. The one limitation of this measurement has been that the cross section determined by these techniques is a quasi total collision cross section which is dependent on the resolution of the system. However, completely classical techniques have been successfully used to analyze the total collision cross-section information to determine the magnitude of the charge exchange contribution. These techniques are outlined in detail in Appendix I, which is a reprint of the paper presented at the IEEE Thermionic Converter Specialist Conference, in Cleveland, Ohio, on October 26 to 28, 1964. One other essential feature that this analysis of the cross-section information has pointed out is the importance of determining ion mobilities

by integrating the diffusion cross section over the ion energy distribution rather than using a value of the diffusion cross section which corresponds to the temperature of the ion energy distribution to determine ion mobility.

Description of the Experiment

Below an ion energy of several electron volts, beam techniques are seriously limited by uncertainties in the determination of the ion beam energy due to contact potential effects which are particularly significant in cesium environments. In the measurement of the total collision cross section of cesium ions interacting with cesium atoms conducted in a modified Ramsauer beam experiment, the problem of contact potential effects was eliminated by employing an electroformed collision chamber. Shown in Fig. 1 of Appendix I is a schematic diagram of the system. Three points of restraint, defined by the entrance and exit slits and the necked-down portion of the collision chamber, uniquely define the radius of a circle. A magnetic field applied perpendicular to the plane of the figure is used to energy select ions produced by contact processes at the porous tungsten cap. Re-entrant type geometry was employed at both the exit and entrance slits of the collision chamber to prevent perturbations of the electric field within the chamber produced by fields in other parts of the apparatus. By electroforming the collision chamber of copper, metal interfaces which can give rise to possible contact potential or thermoelectric effects were eliminated from the inner surface of the chamber. The grain size of the copper plate on the inner surface of the chamber was controlled so that the average grain diameter was on the order of several microns. Therefore, electric fields produced by inhomogeneities in the surface structure do not penetrate into the chamber over dimensions significantly greater than several microns, whereas the length scale of the chamber is on the order of millimeters. The collision chamber was located in an isothermal block to eliminate possible thermoelectric effects produced by temperature variations. Therefore, by using these techniques, a field-free region was created inside the collision chamber. The energy of the ion beam exiting the collision chamber was uniquely determined by measuring the magnitude of the applied magnetic field and knowing the radius of curvature defined by the geometry of the chamber. Only if extreme care is taken to eliminate contact potential effects can the uncertainty in the determination of the ion beam energy be eliminated. To obtain an estimate of the magnitude of the uncertainty in the determination of the ion beam energy caused by contact potential effects, beam energies determined with the electroformed collision chamber system were compared to ion beam energies inferred by measuring the potential difference between the ionizer cap and ion collector. This latter technique, which is subject to contact potential effects, was found to produce as much as 2.5 eV error in the true ion beam energy. The detailed results of these investigations are presented in Ref. 5.

The total collision cross section is determined by measuring the attenuation of the ion beam exiting the collision chamber produced by increases in cesium pressure within the collision chamber. This can be represented by the following

equation

$$I = I_0 e^{-p_0 P_t x} \quad (1)$$

where

- I is the ion beam current exiting the collision chamber for a finite pressure in the chamber
- I_0 is the ion beam current exiting the collision chamber for zero pressure in the chamber
- p_0 is the pressure in the collision chamber reduced to 273°K
- P_t is the number of collisions per cm of path per mm of pressure
- x is the path length of the ion beam through the chamber

From the geometry of the system, scattering events which produced deflections greater than 0.0074 radians were counted. The cross section determined in this manner is composed of elastic scattering events, which produce deflections greater than 0.0074 radians, and all charge exchange reactions. All charge exchange reactions are counted because of the fact that when the ion and atom have exchanged identities, the ion has assumed the energy of the atom which causes the newly formed ion to have an incorrect trajectory in the magnetic field to exit the collision chamber.

By using completely classical techniques as outlined in Appendix I, it is possible to determine the classical differential scattering cross section due to a polarization interaction. Once the classical differential scattering cross section is known, it is possible to determine the value of the actual elastic scattering cross section. The charge exchange cross section can then be determined by subtracting from the measured total collision cross section the contribution due to elastic scattering events. To predict the actual elastic differential scattering cross section by a completely classical analysis, the resolution of the system must be greater than the quantum mechanical cutoff angle. For systems with resolutions below the quantum mechanical cutoff, the uncertainty in the position of the particle is greater than the resolution of the system, and therefore, the cross-section information cannot be interpreted on an entirely classical basis. For the present cesium cross-section measurements over the energy range of 0.12 to 9.7 eV, the resolution of the system is greater than this critical cutoff angle, and therefore, a completely classical analysis of the data is valid. Shown in Fig. 2 of Appendix I is the differential scattering cross section for both elastic and charge exchange events predicted on a classical basis. The finite cutoff at small angles is due to the resolution of the experimental system. The cutoff at large angles for charge exchange interactions corresponds to the angle of scatter produced by the maximum impact parameter at which a charge exchange interaction can take place. The maximum charge exchange cutoff angle, as shown by Sheldon,⁶ is energy dependent. Therefore, the energy dependence of the high-energy charge exchange information must be employed in order to predict this angle. However, in the analysis of the measured total collision cross-section information, the magnitude of the charge exchange cross section can

be determined by subtracting the contribution due to elastic scattering events from the measured total cross section. The only physical parameter that must be utilized in the analysis is the polarizability of cesium which is well-known from the measurements of Salop, et al.⁷

The resolution of the collision chamber has been chosen in a range in which a small inaccuracy in the determination of the resolution of the system does not produce significant changes in the magnitude of the predicted elastic scattering cross section. For systems with higher resolution or with the ability to detect scattering events which produce extremely small deflections, the magnitude of the elastic scattering cross section predicted on a classical basis is extremely sensitive to very small deviations in the scattering angle since on a classical basis the differential cross section becomes infinite for zero angle of deflection.

Once the charge exchange cross section has been determined, as shown in Fig. 5 of Appendix I, it is possible to determine the momentum transfer cross section which is the essential parameter in the analysis of the ion mobility. It has been shown by Holstein and Dalgarno⁸ that the diffusion cross section of an ion moving in its parent gas is twice the cross section for the resonance charge transfer process. In the low-field limit the mobility, μ , can be determined by the expression derived by Holstein⁹

$$\mu = \frac{3\sqrt{\pi}}{8} \frac{e}{\sqrt{mKT}} \frac{1}{N\bar{Q}} \quad (2)$$

where m is the ion mass

N is the neutral density

K is Boltzmann's constant

and

$$\bar{Q} = \frac{1}{2(KT)^3} \int_0^\infty \epsilon^2 \sigma_D e^{-\epsilon/KT} d\epsilon \quad (3)$$

\bar{Q} is the average diffusion cross section which is determined by averaging the diffusion cross section over the ion energy distribution. Therefore, in order to properly evaluate the cesium ion mobility for conditions typical of the cesium plasma in the converter the average diffusion cross section must be determined by averaging the diffusion cross section over the ion energy distribution. This implies that the energy dependence of the diffusion cross section must be known in order to accurately calculate the cesium ion mobility. There has been some question as to the validity of using the low-field approximation in calculating an ion mobility which will be applicable to converter conditions. From electrostatic probe measurements¹⁰ average fields existing in the plasma range from 300 to 1500 volts/mm. For high-pressure converters (approx. 1 mm) the energy gained from the electric field by the ions between collisions is small in comparison to the mean thermal energy of the ion. In this case the use of the low-field approximation is valid. However, in low-pressure converters (10^{-2} mm) the energy gained from the electric field between collisions can be significant due to the increased ion mean free path at these pressures, and therefore, extreme care must be used in applying the low-field

approximation to predict ion probabilities in this case.

Measurements and Results

The principal problem in extending the energy range of the cross section measurements below 0.1 eV is that the detectable ion current level in the system at these energies is below 10^{-18} amps. At this current level the ion beam can be characterized as a series of random pulses, and therefore, dc techniques cannot be used to accurately measure the ion arrival rate. An electron multiplier with beryllium copper dynodes is used to amplify the ion beam current signal level by a factor of 10^5 to 10^6 . Beryllium copper was chosen for the dynodes of the multiplier, since stability rather than extremely high gain is essential in the detection system. Every ion that arrives at the multiplier produces an output of approximately 10^5 - 10^6 electrons. Using sampling oscilloscope techniques, the time-energy characteristics of the multiplier output have been measured. Shown in Fig. 1 is a typical time-pulse distribution of the multiplier output which indicates a pulse half width of approximate 10^{-8} seconds. The pulse distribution of the multiplier output, as would be expected, is Gaussian. A tunnel diode preamplifier circuit is used to amplify and change the nature of the output of the multiplier to a form that can be directly detected with an electronic counter. The stability of the preamplifier circuit, which is usually the major problem in using this type of system, has been found by measurements to be constant for periods on the order of days if the temperature of the circuit is maintained constant. The preamplifier system stability, therefore, is more than suitable for use in measuring lower energy ion cross sections. This circuit has been successfully used to date to detect ion current levels as low as 1.9 ions/min \pm 0.212 with a background count of 0 \pm 0.0. However, further investigations of the system have indicated that background noise can significantly perturb the counting rate. By cutting off the low-energy sensitivity of the preamplifier, it has been possible to eliminate the background noise contribution to the signal. By using this technique, however, a significant portion of the information available is also lost. This loss is not critical in the interpretation of the cross-section measurements, since the cross section is determined by measuring the relative attenuation of the ion beam and not the absolute magnitude of the ion beam current. At extremely low-current levels, however, any loss of significant information results in an increase in the counting time required to make the measurements and also an increase in the lower energy limit at which meaningful measurements can be obtained. Therefore, significant effort has been devoted to reducing the noise level of the system and also to improvement of the ion optics of the deflection system used in conjunction with the multiplier.

Since the preamplifier, which is used to change the output characteristics of the multiplier to a form that can be detected directly with an electronic counter, requires a finite reset time of approximately 10^{-6} sec after the detection of an ion, an upper limit on the ion current level detectable with this system exists. Essentially, this limit is the point at which the average time between ions arriving

at the multiplier becomes comparable to or less than the reset time of the pre-amplifier. Below this upper current level limit, the multiplier count rate should exhibit a linear dependence with current arrival rate. The preamplifier system has been designed so that both a dc electrometer and counter can be used simultaneously to compare the performance of both systems at the higher current levels. Shown in Fig. 2 is the comparison between the count rate and the current level measured with a dc electrometer. Below current levels of 7.5×10^{-14} amps a linear behavior between the count rate and the dc current level has been detected over three orders of magnitude as shown in this figure. The lower limit of this comparison is caused by the limits of the electrometer system. The linear dependence serves to indicate that the preamplifier system is performing correctly and not, for example, double counting over portions of the current range.

In the course of improving the optics of the multiplier deflection system to increase sensitivity, it was found that focusing potentials required to deflect ions into the multiplier were significantly greater than those used in the original cross section measurements. Subsequent investigation of this difference using electrical analogue techniques indicated that a Faraday cage collector system used in the original measurements, but not in these latest tests, changed the shape of the electric field produced by the deflection plates of the multiplier significantly. Experimental measurements employing the Faraday cage collector were conducted to verify this result. Shown in Fig. 3 is the difference in ion current detected by the multiplier as a function of voltage applied to the deflection plate system for systems with and without the Faraday cage collector present. As predicted by the analogue measurements, less applied voltage to the multiplier deflection plates is required when the Faraday cage collector is present in the system to shape the electric field. Also as shown in Fig. 3, the current to the multiplier is constant over approximately 100 volts for the Faraday cage collector system, and the applied voltage to the deflection plates is significantly less than the applied voltages required without the Faraday cage collector system present. The relatively constant ion current to the multiplier over a variation of approximately 100 volts in applied voltage to the deflection plates is due to the finite resolution of the optics of the multiplier system. This result was also predicted from the analogue analysis. The most significant result is that higher ion current levels were detected in the system with the Faraday cage collector present even though in the system without the Faraday cage collector potentials as great as a factor of 20 higher were applied to the deflection plates. Even though the shaping of the field by the presence of the Faraday cage collector was fortuitous, this technique will be used in the future to limit the magnitude of the voltage applied to the deflection plates required to focus the ion beam into the multiplier. With this technique the focus of the system can be improved at lower applied voltage levels which reduces problems associated with voltage breakdown.

As has been indicated previously, a significant effort has been made to

reduce the noise level of the multiplier deflection system. This work has served to eliminate thermionic emission effects produced at the dynodes of the multiplier as one of the causes of the measured background level. It has been found that there is a strong frequency correlation of the background signal level. Therefore, further work has been in progress in this area to eliminate this background level from the system.

Outline of Research for the Next Six-Month Period

1. Studies will be continued to further develop the classical techniques which are used to analyze the total cross section data.
2. Further studies will be made to reduce the background level detected by the multiplier so that the cross section measurements can be extended to energies significantly below energies of 0.1 eV.
3. The total collision cross section will be measured at energies below 0.1 eV, and further information will be obtained at higher energies to verify the existing results.

ELECTRON-CESIUM ATOM COLLISION PROBABILITY MEASUREMENTS

Introduction

Electron-atom collisions play a dominant role in determining the transport properties of slightly and partially ionized plasmas. As a result, a knowledge of the electron-cesium atom collision cross section or collision probability is a prerequisite for an understanding of the properties of the non-equilibrium plasma that exists in the thermionic converter and other plasma devices employing cesium vapor in an ionized state. In most practical cesium plasma devices, electron energies are less than 1 eV. In this range of electron energies there is approximately an order of magnitude variation in the experimental cross-section values with no particular energy dependence exhibited in the reported data. Consequently, it has become common practice, when making calculations pertaining to the analysis of a particular device, to use what appears to be a reasonable average of the existing cross-section data or to use a value which has been inferred from the operational characteristics of a cesium plasma device, such as the thermionic converter. Such procedures can lead to significant errors.

The acute need for accurate data pertaining to electron-cesium atom collisional processes has prompted this investigation of the elastic electron-cesium atom cross section for momentum transfer. Momentum transfer collisions are significant in the determination of such parameters as electron mobility, conductivity, and drift velocity. Earlier measurements of the electron-cesium atom cross section for momentum transfer over an energy range from 0.05 to 0.1 eV were conducted under Contract NASr-112 using electron cyclotron resonance techniques. Since the upper energy limit of the cyclotron resonance technique in cesium vapor was found to be 0.1 eV, the collision probability measurements in the present investigation over an energy range from 0.1 - 0.5 eV are being conducted in the positive column of a cesium arc discharge. Measurements of plasma properties are made using electrostatic probes and rf conductivity probing techniques. An effective electron-cesium atom collision frequency for momentum transfer is obtained experimentally, and from this information the magnitude and velocity dependence of the cross section is determined through an appropriate integral analysis.

Theory and the Plasma Model

The equation describing the electron current flow through a gas under the influence of an applied dc electric field may be derived on the basis of the physical model for a plasma originally developed by Lorentz. In this approach, it is assumed that collisions are instrumental in setting up a nearly spherically symmetric velocity distribution of electrons and that small deviations from spherical symmetry are described accurately enough by the second term in the spherical harmonic expansion of the velocity distribution function. Upon

substitution of this first order expansion into the Boltzmann equation, two coupled equations describing the relationship of the terms of the expansion result. From this relationship and the equation for particle current, the following equation may be obtained

$$J = -\frac{4\pi}{3} \frac{n_e e^2}{m} \int_0^\infty \frac{v^3 (\partial f_0 / \partial v)}{\nu_{eo}(v) + \nu_{ei}(v)} dv E, \quad (4)$$

where

m - electron mass

e - electronic charge

v - electron velocity

n_e - electron number density

J - current density

E - electric field intensity

f_0 - isotropic part (first term in spherical harmonic expansion) of the velocity distribution function normalized with respect to electron density

$\nu_{eo}(v)$ - elastic electron-atom collision frequency for momentum transfer

$\nu_{ei}(v)$ - appropriate electron-ion collision frequency for momentum transfer

In this derivation it has been assumed that the plasma is uniform, that the collisional friction force exerted on electrons is due to momentum transfer encounters with heavy particles, and that electron-electron encounters have no direct influence on the momentum of the electron gas. A complete analysis of the problem, which yields this result, is presented in Ref. 11.

If it is assumed that electron-electron collisions are influential in establishing a Maxwellian distribution of electron velocities and that electron-ion collisions can be neglected in comparison to electron-atom collisions, Eq. 4 becomes

$$J = \frac{8}{3\sqrt{\pi}} \frac{n_e e^2}{m} \left(\frac{m}{2kT_e} \right)^{\frac{5}{2}} \int_0^\infty \frac{v^4 e^{-\frac{mv^2}{2kT_e}}}{\nu_{eo}(v)} dv E, \quad (5)$$

which can be expressed in the convenient form

$$J = \frac{n_e e^2}{m \nu_{eff}} E, \quad (6)$$

where ν_{eff} , the effective collision frequency, is given by

$$\nu_{eff}^{-1} = \frac{8}{3\sqrt{\pi}} \left(\frac{m}{2kT_e} \right)^{\frac{5}{2}} \int_0^\infty \frac{v^4 e^{-\frac{mv^2}{2kT_e}}}{\nu_{eo}(v)} dv. \quad (7)$$

The collision frequency is related to the momentum transfer cross section through the following relationship

$$\nu_{ea}(\nu) = n_a Q_{ea}(\nu) \nu, \quad (8)$$

where

n_a - atom density

$Q_{ea}(\nu)$ - elastic electron-atom momentum transfer cross section

Substituting this form into Eq. 7 and normalizing the collision frequency with respect to atom density, n_a , yields

$$\nu_{eff}^{*-1} = \left(\frac{\nu_{eff}}{n_a} \right)^{-1} = \frac{8}{3\sqrt{\pi}} \left(\frac{m}{2kT_e} \right)^{\frac{5}{2}} \int_0^{\infty} \frac{v^3 e^{-\frac{mv^2}{2kT_e}}}{Q_{ea}(\nu)} dv, \quad (9)$$

Eq. 9 represents the product of cross section and electron velocity properly averaged over-all electron velocities and is a function of electron temperature only. It should be noted that the effective collision frequency defined by the preceding equations is not the "average" collision frequency but rather a parameter defined for convenience which pertains only to this particular formulation of the problem. This parameter, however, if known as a function of electron temperature, would be extremely useful in the calculation of dc plasma transport properties.

It is apparent from Eq. 9 that knowledge of the normalized effective collision frequency electron temperature dependence could lead to a determination of the cross section which appears in the denominator of the integrand. A numerical trial function analysis for the cross-section velocity dependence has been carried out using Eq. 9 and will be presented in another section.

Using the perfect gas relationship

$$n_a = \frac{P}{kT_a}, \quad (10)$$

where

P - cesium vapor pressure

k - Boltzmann's constant

T_a - cesium gas temperature

along with Eq. 6, the following equation can be obtained

$$\nu_{eff}^* = \frac{e^2 k}{m} \cdot \frac{n_e E A}{(P/T_a) I}, \quad (11)$$

where

A - cross sectional area of the plasma sample

I - current passing through plasma sample

This equation relates the effective normalized electron-atom collision frequency, which is a function of electron temperature only, to the other measurable parameters of the plasma system, namely, electron density, electric field, gas temperature and pressure, and current.

Description of the Experiment

The laboratory plasma used in this investigation is the positive column of a cesium arc discharge which is a relatively quiescent plasma having a controllable degree of ionization, low electron temperature, and consequently nearly thermal distribution of electron velocities. The theoretical model previously outlined is used to describe the cesium arc discharge plasma which has properties similar to those encountered in practical cesium plasma devices but is more suitable for laboratory diagnosis. For moderate pressures (10^{-2} - 10^{-1} mm Hg) and currents (0.3 - 1.5 amps), the degree of ionization in the positive column of the discharge varies from about 10^{-4} to 10^{-2} while the electron temperature varies from approximately 2500 to 4500°K. The electron density in the plasma is uniform axially and circumferentially, while gradients due to diffusion exist in the radial direction. There are no plasma density gradients parallel to the axially applied dc electric field and, consequently, the plasma behaves as though it were nearly uniform. A simple averaging process can be used to account for the radial variation in electron density (see Appendix II). As a result of the uniform characteristics of the cesium plasma of the positive column of the discharge, the plasma is amenable to analysis. This is in contrast to the conditions existing in the arc mode thermionic converter in which severe gradients in plasma properties exist.

Of the parameters in Eq. 11 required to experimentally obtain the normalized effective collision frequency, the electron density and temperature are the two most difficult to measure experimentally. Of the various plasma diagnostic techniques available, the most practical for this purpose is the electrostatic probe. From an analysis of the current voltage characteristics of an electrostatic probe, the electron temperature and density can be determined and the assumption regarding the equilibrium distribution of electron energies verified. In addition, the electric field can be determined from plasma potential measurements made with probes positioned axially along the positive column. A high degree of spatial resolution can be realized with electrostatic probes, and they can be moved from point to point in the plasma to measure local conditions.

As a check on the potential measurements made with electrostatic probes and the discharge current measurements, rf conductivity probes are used to measure the plasma conductivity. In this technique, a small probing rf coil is inserted in the plasma. The magnetically induced rf electric field of the coil penetrates into the plasma which behaves as a lossy medium for the rf power, loading the coil to an extent determined by the plasma conductivity. Therefore, a measurement

of the power dissipated can be directly related to the plasma conductivity. These measurements provide an independent check on the experimentally determined ratio of current density to electric field.

A photograph of a typical discharge tube is shown in Fig. 4. Cathode to anode separation in this tube is 50 cm, and the inside diameter is 3.8 cm. The electrostatic probe sidearm assemblies shown in the photograph are constructed in such a way that the probes, which protrude through a small hole in the wall of the discharge tube, can be moved radially into the plasma. The probes are constructed of 0.010-in. diameter tungsten rod with a glass sheath used as an electrical insulator around the sidewall. The entire assembly, averaging 0.017 in. in diameter, is ground flat, exposing only the .010-in. tungsten tip to the plasma. Several probes are used with each tube and are positioned at 8-cm intervals along the tube axis. During operation the tube is located within an oven which controls the gas temperature and prevents cesium from condensing on the tube walls. The appendix shown in the figure extends down to a lower oven which is always held at a lower temperature than the main oven in order to control the cesium vapor pressure. Fig. 5 shows a tube designed for use with the conductivity probe. The conductivity probe shown in the figure is inserted axially through a hole in the anode. Fig. 6 is a detailed view of the anode area of this tube. The probe coil in this photograph contains about 20 turns of 0.010-in. gold wire and is approximately 0.25 in. long.

Measurements and Results

Typical experimental measurements are conducted with cesium pressure and discharge current as independent variables. All other plasma properties are established by fixing these two parameters. A high degree of stability in the discharge current is achieved by using a high-regulation dc power supply. The cesium pressure is determined from the cesium vapor pressure curve of Ref. 12 and is a strong function of temperature. Consequently, stabilization and control of the temperature in the pressure control oven containing the cesium reservoir is critical. The temperature in this oven, which is varied from 150 - 200°C in order to achieve the range of pressures of interest, is controlled by a temperature stabilization circuit capable of holding the oven temperature to within $\pm 1/2^\circ\text{C}$. The sensing element for the circuit is a commercially available platinum wire resistor and is in close contact with the liquid cesium in the appendix. Cesium reservoir temperature is measured with two precision grade laboratory thermometers which have been calibrated by the manufacturer against a standard that has been calibrated at the NBS. These thermometers are certified accurate to $\pm 1/8^\circ\text{C}$. Temperature gradients inside the oven are effectively eliminated by circulating the air with a fan.

The electron temperature, electron density, and plasma potential variations in the discharge are measured using pulsed, electrostatic probe techniques. A

pulsing system is used to apply a cleaning pulse, sweep voltage or data acquisition pulse, and rest voltage to the probe. The time duration of each portion of the probe pulse can be varied independently. The time scale of the total pulse applied to the probe with this system ranges from approximately 100 microseconds to 100 milliseconds. With such versatility, the effect of changing probe surface conditions, errors due to circuit and plasma response limitations, and the effect of plasma drift or instability can be detected. The importance of being able to vary sweep speed and applied voltage in this manner is detailed in Ref. 13 and 14.

Conductivity probing techniques are currently being used as a check on the measured ratio of current density to electric field. The probe, which is inserted along the tube axis (see Fig. 5) in order to take advantage of the common symmetry of the probe and the discharge, detects the conductivity in its immediate vicinity by dissipating a very small amount of radio frequency (10 mc) power in the plasma. This weak interaction with the plasma is detected by observing the resistive loading of a sensitive oscillator-detector. The loading is then compared with a calibration curve obtained by placing the probe in a variety of salt solutions having known conductivities. From such a comparison the conductivity of the plasma can be determined. Probes of this type are very sensitive to temperature change and must be temperature corrected by determining the amount of energy dissipated in known resistive loads at the temperatures the probes will encounter in operation (200 - 300°C). The amount of energy dissipated at operating temperature is then compared to the amount dissipated at room temperature for a fixed resistive load. From this information, a temperature correction is applied to the salt solution calibration curve so that temperature effects may be distinguished from those due to real power dissipation in the plasma. Electrostatic probes are positioned in the region of the conductivity probe so that the electric field can be determined in the portion of the discharge tube occupied by the conductivity probe well. From the electric field and discharge current measurements, an independent value of the conductivity is obtained and compared with the rf probe measurements. Fig. 6 shows the relative positioning of conductivity and electrostatic probes. A complete description of the rf probe and its associated instrumentation is presented in Ref. 15 and 16.

A typical radial profile of electron density is presented in Fig. 7 as a function of discharge current for a fixed cesium pressure. The measurement is made by moving the electrostatic probe along its sidearm (see Fig. 4 and 5) with a magnet which is inserted through a hole in the oven wall. Probe characteristics are taken at several positions along the tube radius. The exact position of the probe in the tube is determined by matching a point on the probe to a scale which is positioned parallel to the sidearm. As would be expected, the electron density decreases from a maximum on the axis of the tube to nearly zero at a point close to the wall. This is found to be the case for all currents and pressures checked to date. The experimentally determined electron density profile is compared in Fig. 7 to a simple parabola and a first order Bessel function. In the averaging

of electron density over the cross section, use of either function as an approximation to the experimental data is satisfactory. However, if no correction is made for the density profile, the experimentally determined effective collision frequency can be altered by over a factor of two.

Figures 8-11 present the experimentally determined electron temperature, electron density, electric field, and degree of ionization as a function of discharge current and pressure. As can be seen from Fig. 8, the electron temperature is rather insensitive to pressure but is a strong function of discharge current as the current decreases. This is in agreement with the general trend exhibited by the electric field shown in Fig. 9. The electron temperature is extremely sensitive to fluctuations in the electric field because of the ability of the electron gas to respond instantly to a change in potential. It is for this reason that stability of the applied electric field is critical. In order to increase the range of mean electron energies, efforts have been directed toward operation of the discharge at lower currents where the electron temperature rapidly increases as is shown in Fig. 8. At the present time, operation below 0.3 amps is difficult because the arc becomes unstable. The electron density presented in Fig. 10 is the value measured on the center line of the tube and is seen to be strongly dependent on both discharge current and pressure. From the value of electron density and the atom density calculated from the perfect gas law, the degree of ionization is obtained and plotted in Fig. 11. The degree of ionization is defined as the ratio of electron to atom density. Note that although the absolute value of electron density increases with increasing pressure, the degree of ionization decreases. Because of the radial variation of electron density and the independence of atom density on radius, the degree of ionization varies from its value on the tube axis to the wall in the same manner as the electron density.

According to the theoretical model established in a previous section, the experimentally determined normalized effective collision frequency, Eq. 11, should be a function only of electron temperature and should be independent of both pressure and the degree of ionization. This is the result of assuming that the only electron-heavy particle interactions were electron-caesium atom collisions. From measurements of the various plasma parameters discussed in the previous paragraph and presented in Fig. 8 - 11, the normalized effective collision frequency can be determined from Eq. 11. Shown in Fig. 12 is the experimentally determined variation of the normalized effective collision frequency with electron temperature and degree of ionization. As can be seen from Fig. 12, the data describing the normalized effective collision frequency exhibits a dependence on the degree of ionization indicating that electron-ion collisions are making a noticeable contribution. However, in Fig. 12, a factor of four increase in the degree of ionization has resulted in an increase of only about 40 per cent in the effective collision frequency for a fixed electron temperature. This indicates that a degree of ionization of 10^{-4} is just on the fringe of the region where

electron-ion effects first become important. This point is further illustrated in Fig. 13, in which an electron-heavy particle effective collision frequency was calculated numerically for an assumed electron-cesium atom collision probability velocity dependence. The form of the integral describing the effective collision frequency is a modification of Eq. 9 and includes the effects of electron-ion collisions. The assumed form of the velocity dependent electron-atom cross section used in the calculations is compatible with the cross-section information currently available. The result of using other similar trial functions for the collision probability has been found to yield the same qualitative behavior. The importance of the degree of ionization on the effective collision frequency is determined by the relative magnitude of electron-atom and electron-ion collision cross sections. It is apparent from the experimental and theoretical data presented in Fig. 12 and 13 that for cesium, electron-ion effects first become noticeable for a degree of ionization of approximately 10^{-4} , become significant as the degree of ionization approaches 10^{-3} , and begin to dominate the collisional processes as the degree of ionization approaches 10^{-2} .

Another significant fact which is apparent from Fig. 12 and 13 is that the qualitative behavior of the effective collision frequency is not significantly altered in the temperature range of this experiment as electron-ion effects first become noticeable. The qualitative behavior of the effective collision frequency as a function electron temperature is determined by the velocity dependence of the electron-cesium atom collision cross section, while the effect of electron-ion collisions results only in a shift in the magnitude of the collision frequency. Of course, as the degree of ionization reaches the point where electron-ion collisions dominate, the qualitative behavior of the effective collision frequency is determined by the electron-cesium ion cross section.

Analysis of Trial Functions for the Cross Section

Since the experimental measurements lead to a normalized effective collision frequency, which is averaged over-all electron velocities, it is necessary to determine how the integral describing the collision frequency behaves as a function of electron temperature for variations in the form of the velocity dependence of the collision probability. Numerical integration techniques permit analysis of this integrated behavior for trial forms of the electron-cesium atom collision probability velocity dependence. Various trial forms are selected on the basis of best estimates as to the magnitude of the collision probability and on trends observed in experimental data. These trial forms are then substituted into the integral describing the effective collision frequency, Eq. 9, and numerical integration performed. For the purpose of illustrating the importance of proper averaging of the collision probability, only a few of the seventy-five odd trial functions integrated to date are presented in Fig. 14.

The upper plot in Fig. 14 presents collision probability as a function of electron velocity. The lower curve is the integrated collision probability (effective normalized collision frequency) as function of electron temperature. The trial forms for the collision probability were chosen to coincide with the data obtained in Ref. 17 - 19. Note that the integrated values of curves a and b are almost identical, even though the collision probability variation at lower energies is drastically different for these two curves. On the other hand, when the high-energy end of the collision probability is modified, curve c, the effect on the average is quite significant. Of interest is the fact that the number of electrons in a Maxwellian distribution at a temperature of 2500°K , having velocities less than and greater than the velocities corresponding to the point where the collision probability deviates from the common portion of curves a, b, c, is approximately the same. These velocities are designated by v_1 and v_2 in Fig. 14. However, at 2500°K on the lower curve, the effective collision frequency is unaffected by the low-energy deviation of the collision probability but is effected by the deviation at higher energy. Exactly the opposite behavior could be illustrated by the use of other trial functions. The important point is the fact that integrals of the type describing the effective collision frequency do not necessarily weight the collision probability (cross section) at the most probable electron velocities, as is so often assumed. Occasionally, the collision probability is assumed to be constant and an average value assumed. In Fig. 14, the effective collision frequency is calculated and presented for an assumed constant value of 1400 for the collision probability. The result differs from those previously presented by a factor of 3 at 2500°K , as can be seen from the scale on the right side of the figure, even though an average value of 1400 may seem to be a reasonable estimate for the collision probability curves used in the calculation of effective normalized collision frequency. This and the previous examples serve to point out the importance of proper averaging of the collision probability and the effect that this averaging can have on the determination of the effective collision frequency and plasma transport properties.

Experiments in these low-energy (0 - 1 eV) ranges usually measure a parameter which is similar to the previously defined effective collision frequency (Eq. 9). In order to obtain an effective cross section, the collisional parameter is normalized with respect to atom density and divided by the most probable electron velocity for a given electron temperature. This approach assumes that the heaviest weighting of the integral describing the collisional process occurs at the most probable velocity which is not always true. Of more importance is the fact that the electron temperature variation of the effective collisional parameter is dependent on the theoretical formulation necessary to describe the particular physical system and on the experimental techniques used to measure the properties of the system. The collisional parameter is not a unique plasma property, as is the actual velocity dependent collision frequency, but rather is defined for convenience to represent the over-all effect of collisions on a particular measurement. Consequently, the manner in which the actual collision frequency is averaged

and therefore the measured "effective" collision frequency is dependent on the type of experiment from which the data was obtained. Misunderstanding of this particular point is largely responsible for the lack of agreement in average cross-section measurements in the range of a few tenths of an eV. Only in the case of constant collision frequency (v^{-1} dependence of cross section on electron velocity) do all the effective forms of the collision parameter reduce to the same value and represent the true collision frequency.

Outline of Research for the Next Six-Month Period

1. R.f. conductivity probe measurements will be made so that an independent check on the ratio of current density to electric field can be obtained.
2. Electrostatic probe measurements will be continued in order to determine the normalized effective collision frequency which is used in the determination of the collision probability.
3. Analysis of trial functions, which parallels the experimental program, will be continued with emphasis on the specific detail of the trial functions in an effort to accurately determine the electron-atom cross section for momentum transfer as a function of electron velocity.

REFERENCES

1. J. W. Sheldon, "Mobility of Positive Ions in Their Own Gas: Determination of Average Momentum-Transfer Cross Section," NASA Technical Note D-2408, August 1964.
2. R. M. Kushnir, B. M. Palyukh, and L. A. Vena, Bulletin of the Academy of Sciences, USSR (Physics Series) 23, 995 (1959).
3. C. L. Chen and M. Raether, Phys. Rev. 128, 16, 2679 (1962).
4. L. M. Chanin and R. D. Steen, "Mobilities of Cesium Ions in Cesium" Phys. Rev. 132, 6, 2554-2557 (1963).
5. R. H. Bullis, "Low Energy Cesium Ion-Atom Collision Cross Sections," IEEE Thermionic Conversion Specialist Conference Proceedings, October 7, 8, and 9, 1963, Gatlinburg, Tennessee.
6. J. W. Sheldon, "Cesium Ion-Neutral Scattering and Ion Mobility in the Low Field Limit," to be published in the Proceedings of the Thermionic Conversion Specialist Conference, October 26, 27, and 28, 1964, Cleveland, Ohio.
7. A. Salop, E. Pollack, and B. Bederson, Phys. Rev. 124, 1431 (1961).
8. T. Holstein and A. Dalgarno, Atomic and Molecular Processes (Edited by D. R. Bates, Academic Press, New York, 1962), Chap. 17.
9. T. Holstein, J. Phys. Chem. 56, 832 (1952).
10. R. H. Bullis and W. J. Wiegand, "Characteristics of the Neutralization Plasma in the Arc-Mode Thermionic Converter," to be published in the Proceedings of the Thermionic Conversion Specialist Conference, October 26, 27, and 28, 1964, Cleveland, Ohio.
11. H. Dreicer, Phys. Rev. 117, 343 (1960).
12. W. B. Nottingham, M.I.T. Res. Lab. of Electronics, Quarterly Progress Rept. No. 58, July 15, 1960.
13. R. H. Bullis and W. J. Wiegand, "Probe Measurements in a Cesium Plasma Converter," Proceedings of the Twenty Third Annual Conference on Physical Electronics, M.I.T. (1963).
14. J. F. Waymouth, J. App. Phys., 30, 1404 (1959).

References continued

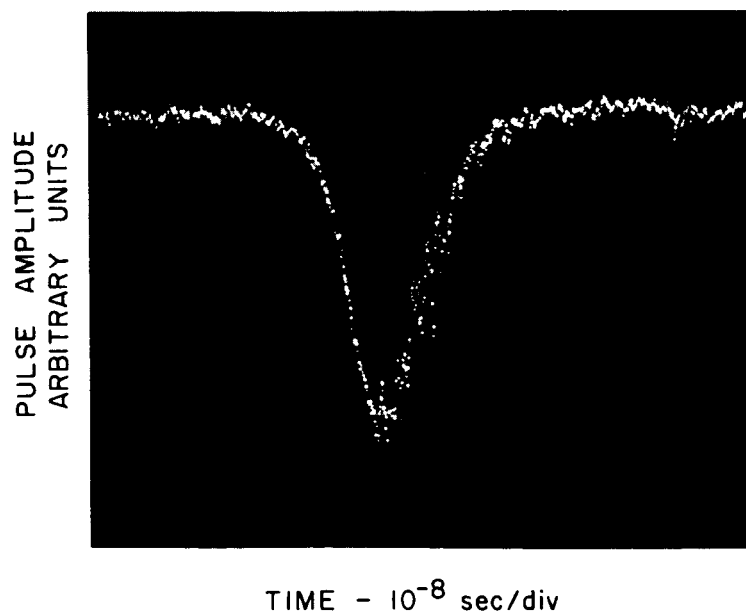
15. E. C. Lary and R. A. Olson, Rev. of Sci. Instr. 33, 1350 (1962).
16. E. C. Lary and R. A. Olson, AIAA J. 1, 2513 (1963).
17. C. L. Chen and M. Raether, Phys. Rev. 128, 2679 (1962).
18. R. K. Flavin and R. G. Meyerand, Jr., "Collision Cross Section of Low-Energy Electrons with Cesium Atoms," Proceedings of the IEEE Thermionic Converter Specialist Conference, Gatlinburg, Tennessee (1963).
19. R. B. Brode, Phys. Rev., 34, 673 (1929).

LIST OF FIGURES

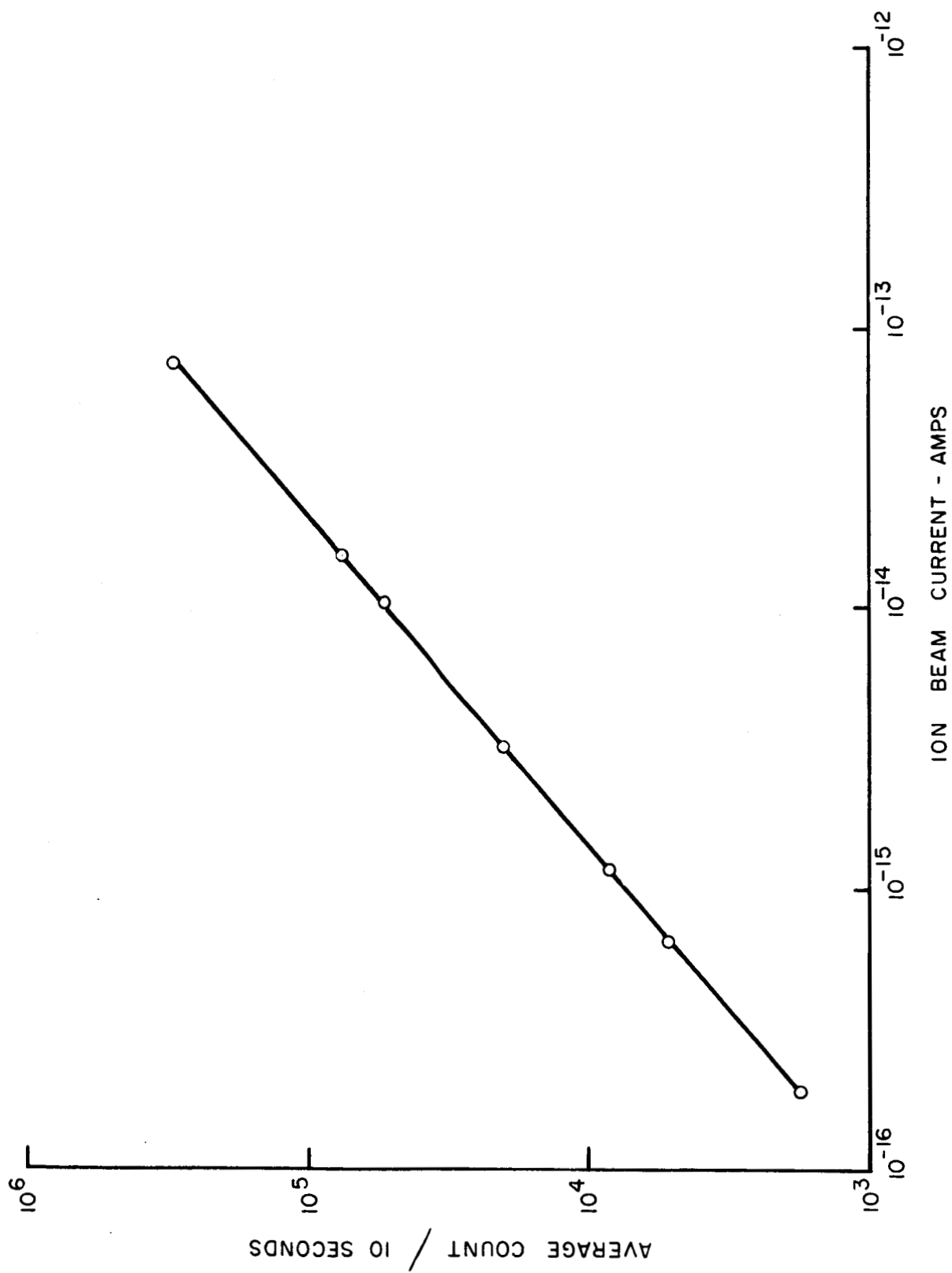
- Fig. 1 - Characteristics of Multiplier Output
- Fig. 2 - Comparison of Count Rate to Electrometer Measurements
- Fig. 3 - Deflection Plate Focusing Characteristics
- Fig. 4 - Cesium Discharge Tube
- Fig. 5 - Cesium Discharge Tube with Conductivity Probe
- Fig. 6 - Anode Region of Cesium Discharge Tube with Conductivity Probe
- Fig. 7 - Variation of Electron Density with Radial Position
- Fig. 8 - Variation of Electron Temperature with Discharge Current and Pressure
- Fig. 9 - Variation of Electric Field with Discharge Current and Pressure
- Fig. 10- Variation of Electron Density with Discharge Current and Pressure
- Fig. 11- Variation of Degree of Ionization with Discharge Current and Pressure
- Fig. 12- Normalized Effective Collision Frequency Variation with Degree of Ionization and Electron Temperature
- Fig. 13- Effective Electron Cesium Heavy Particle Collision Frequency as a Function of Electron Temperature and Degree of Ionization
- Fig. 14- Electron Cesium Atom Collision Probability Variation with Electron Velocity

Normalized Effective Collision Frequency with Electron Temperature

CHARACTERISTICS OF MULTIPLIER OUTPUT



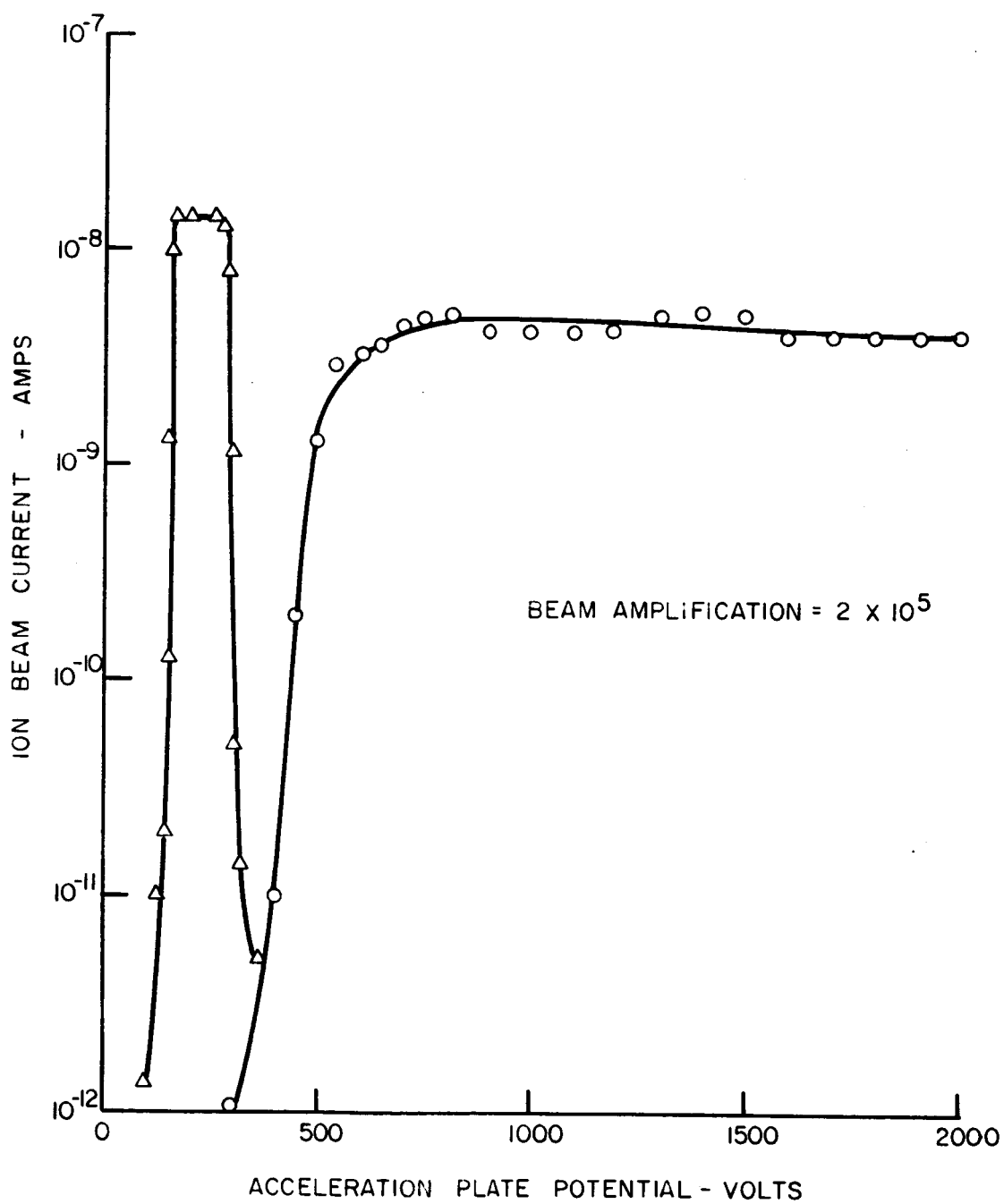
COMPARISON OF COUNT RATE TO ELECTROMETER MEASUREMENTS



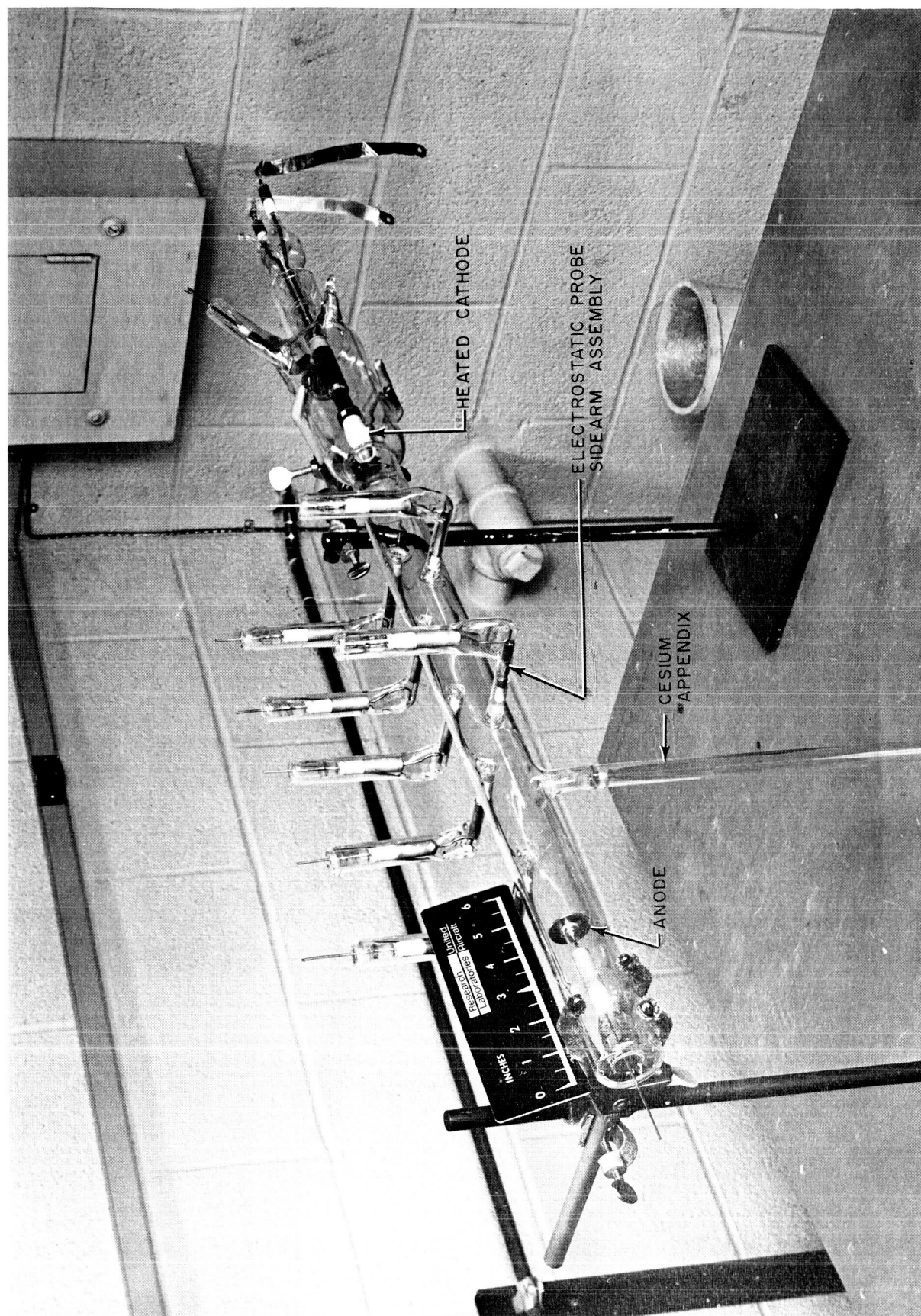
DEFLECTION PLATE FOCUSING CHARACTERISTICS

 Δ WITH FARADAY CAGE COLLECTOR SYSTEM

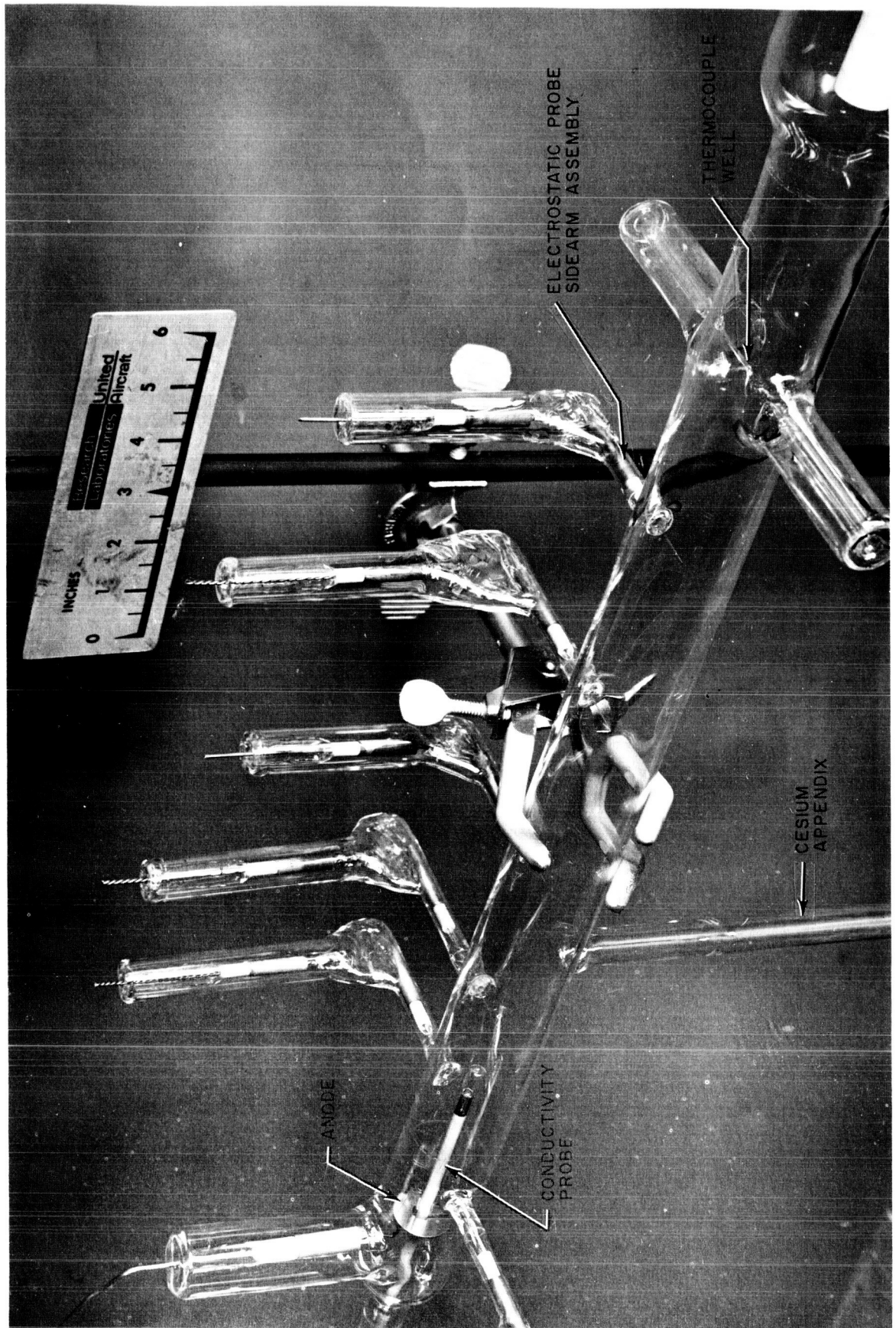
O WITHOUT FARADAY CAGE COLLECTOR SYSTEM



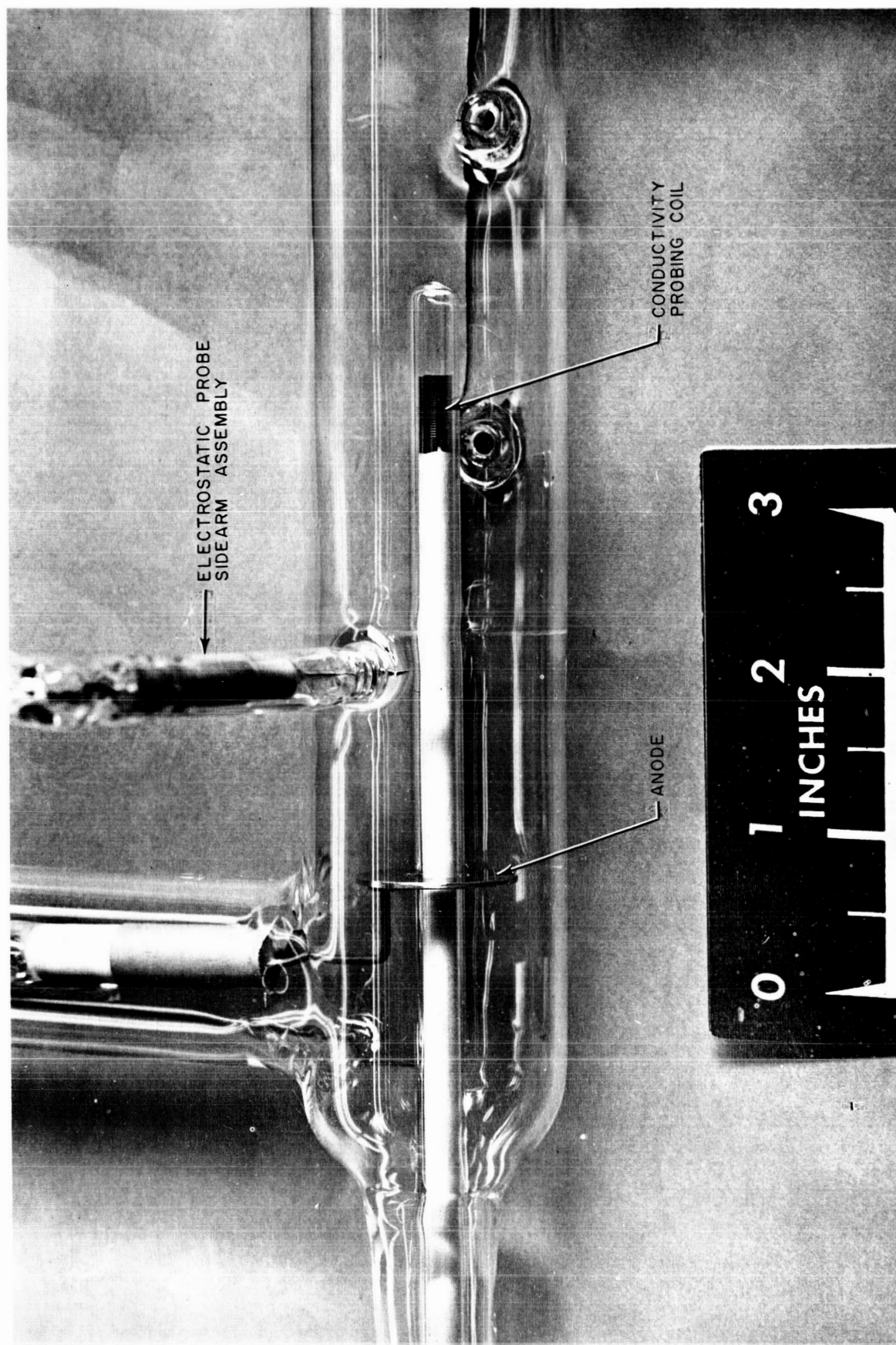
CESIUM DISCHARGE TUBE



CESIUM DISCHARGE TUBE WITH CONDUCTIVITY PROBE



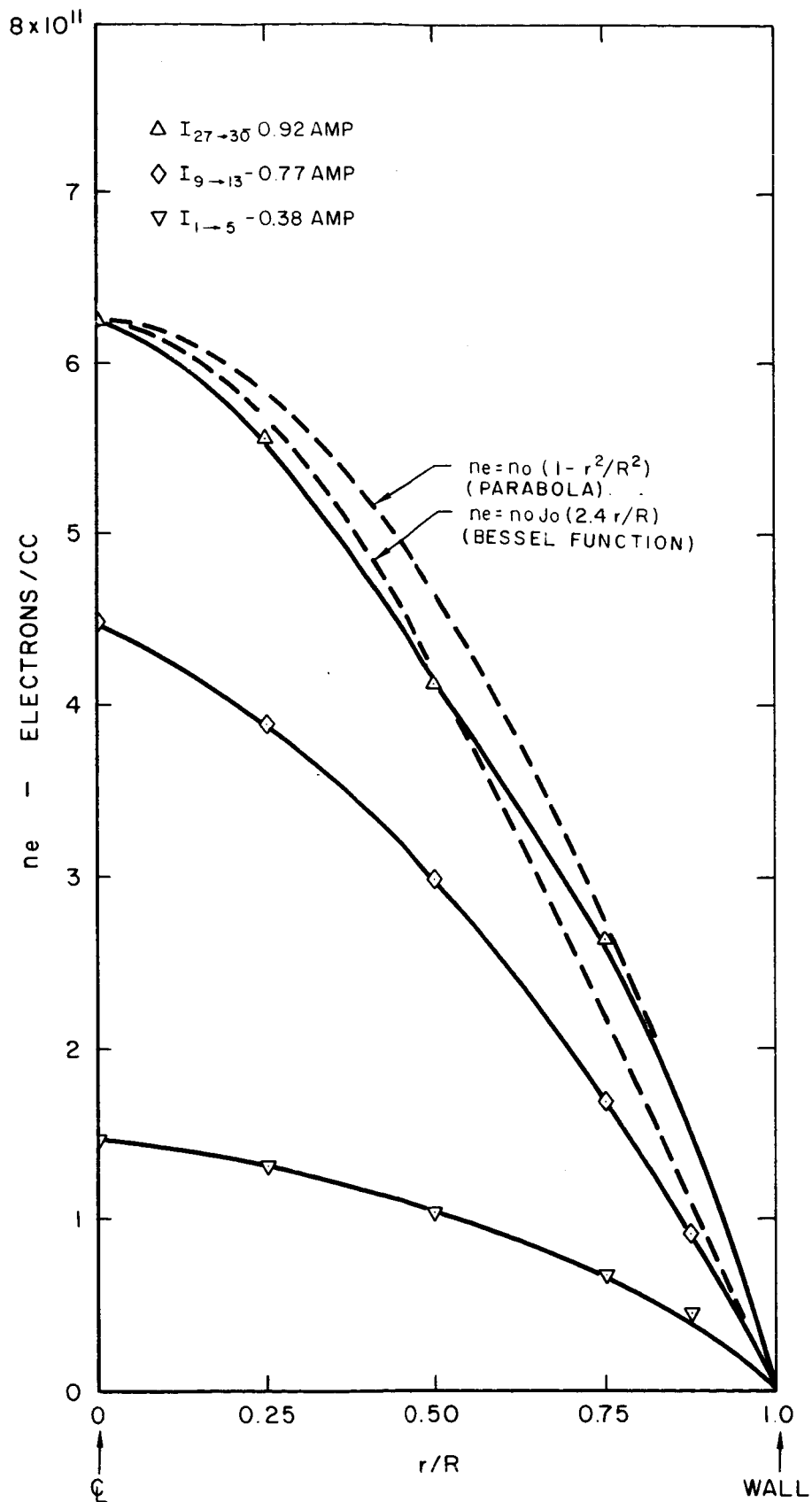
ANODE REGION OF CESIUM DISCHARGE TUBE WITH CONDUCTIVITY PROBE



VARIATION OF ELECTRON DENSITY
WITH RADIAL POSITION

FIG. 7

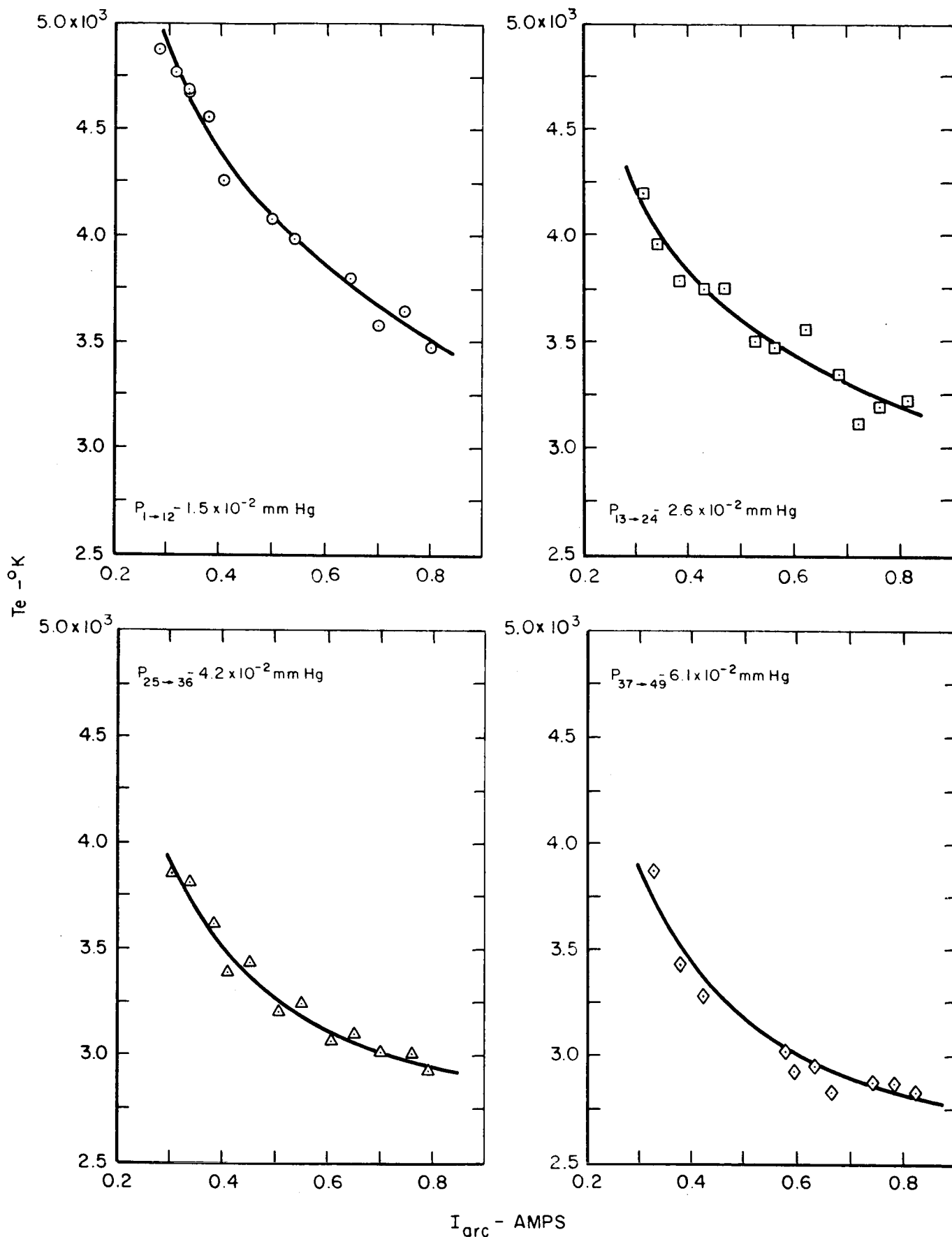
TEST 6-B



VARIATION OF ELECTRON TEMPERATURE
WITH DISCHARGE CURRENT AND PRESSURE

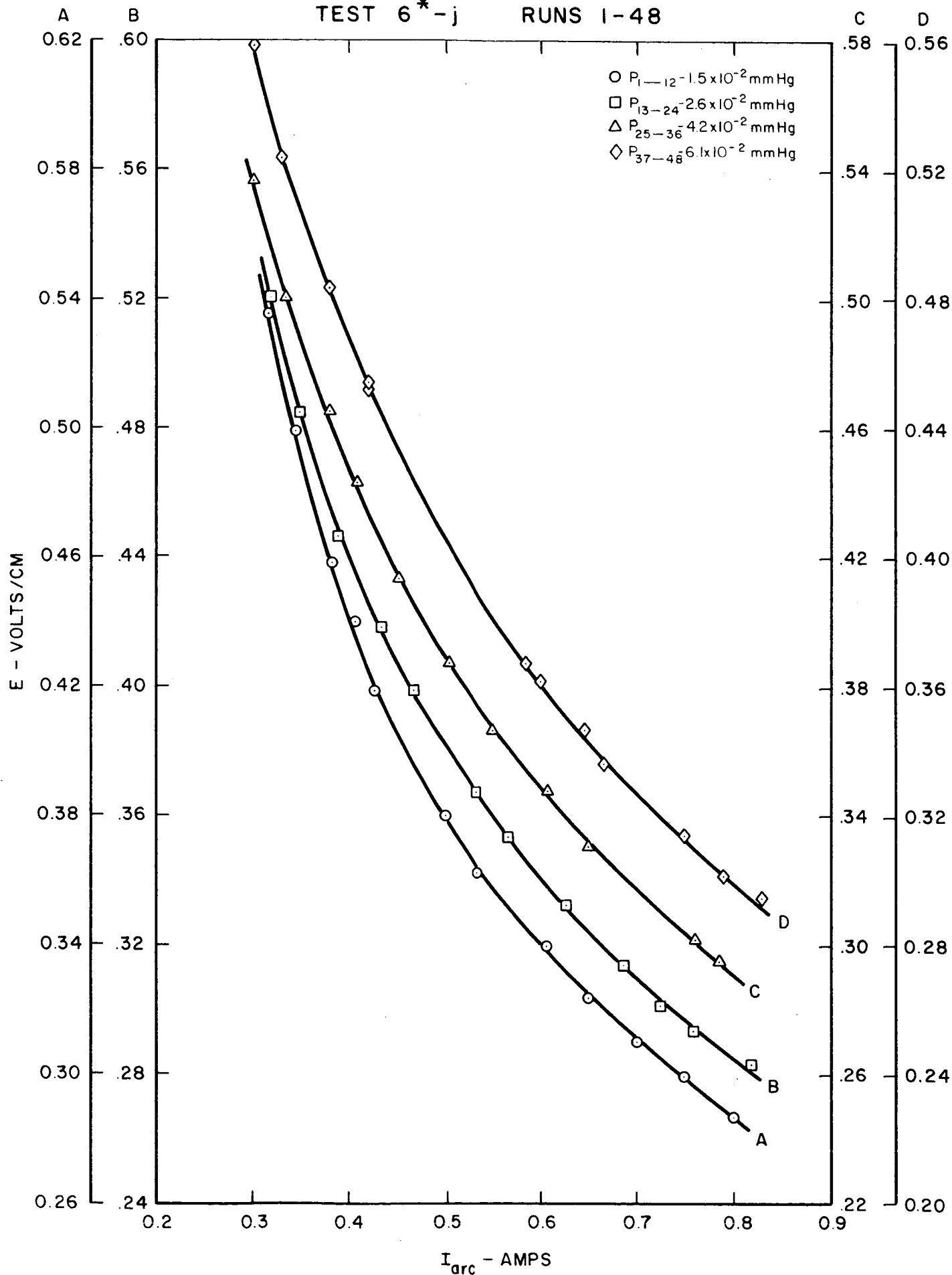
TEST 6*-j

RUNS 1-48



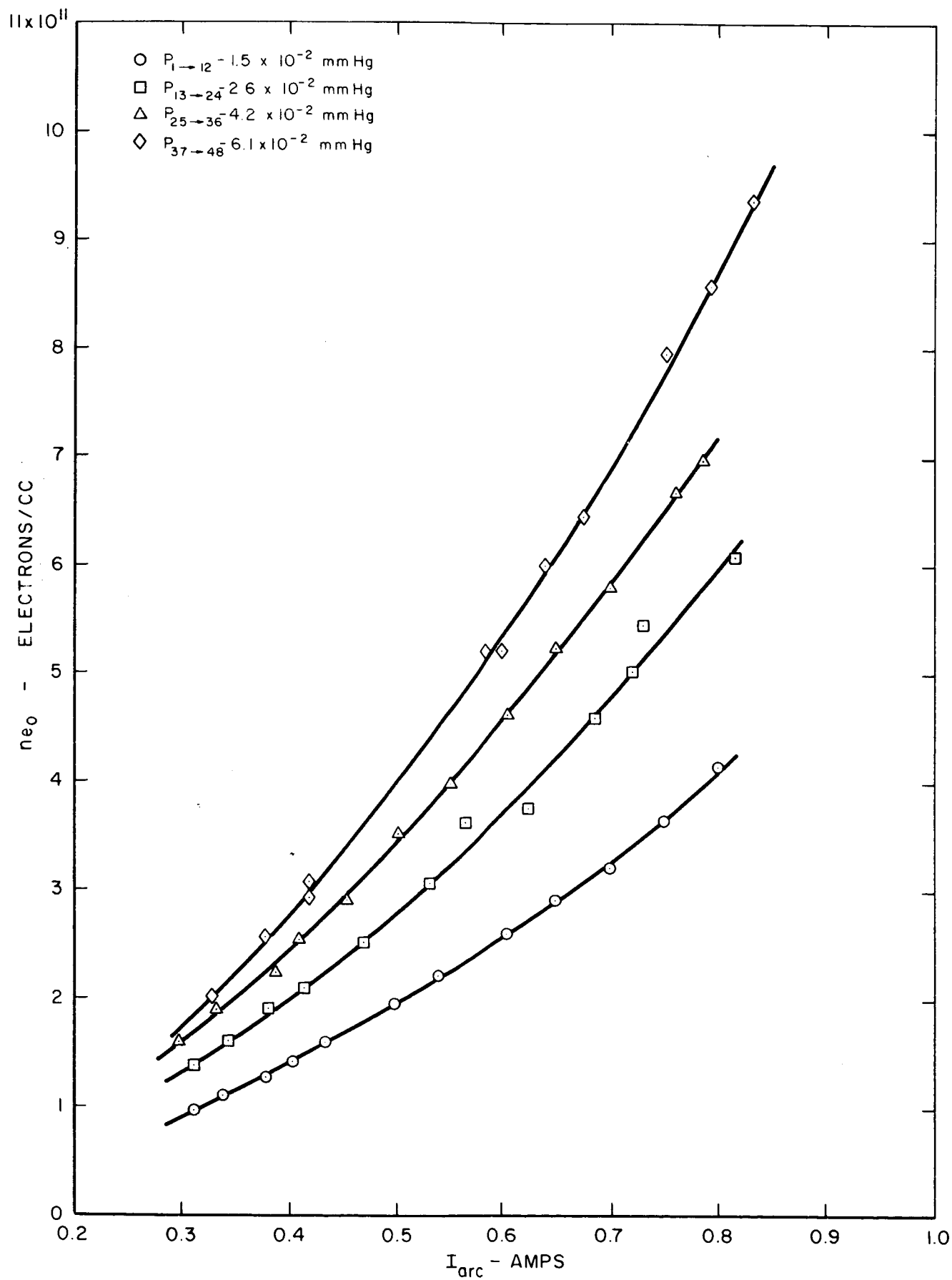
VARIATION OF ELECTRIC FIELD
WITH DISCHARGE CURRENT AND PRESSURE

TEST 6*-j RUNS 1-48



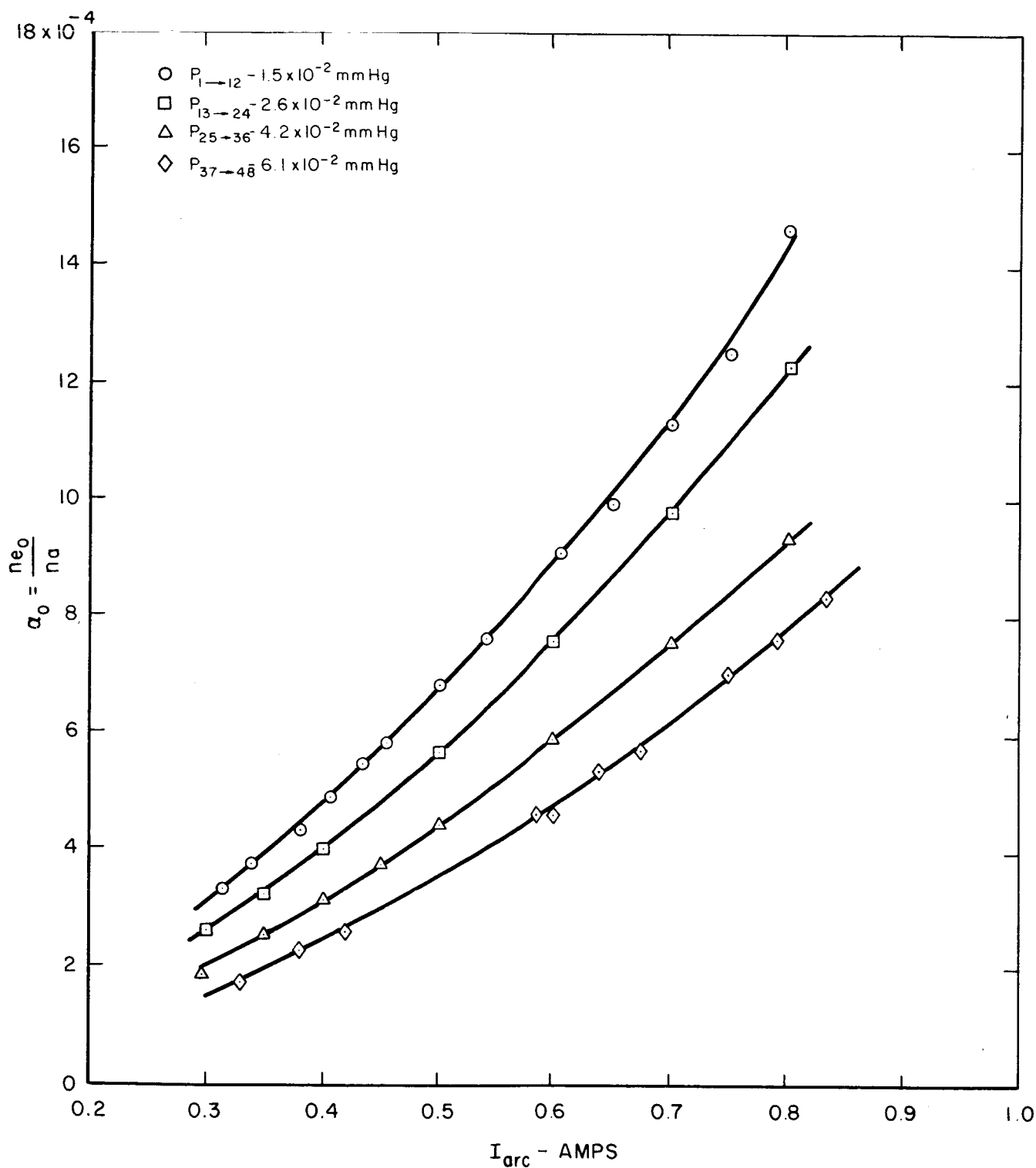
VARIATION OF ELECTRON DENSITY
WITH DISCHARGE CURRENT AND PRESSURE

TEST 6* - j RUNS 1-48



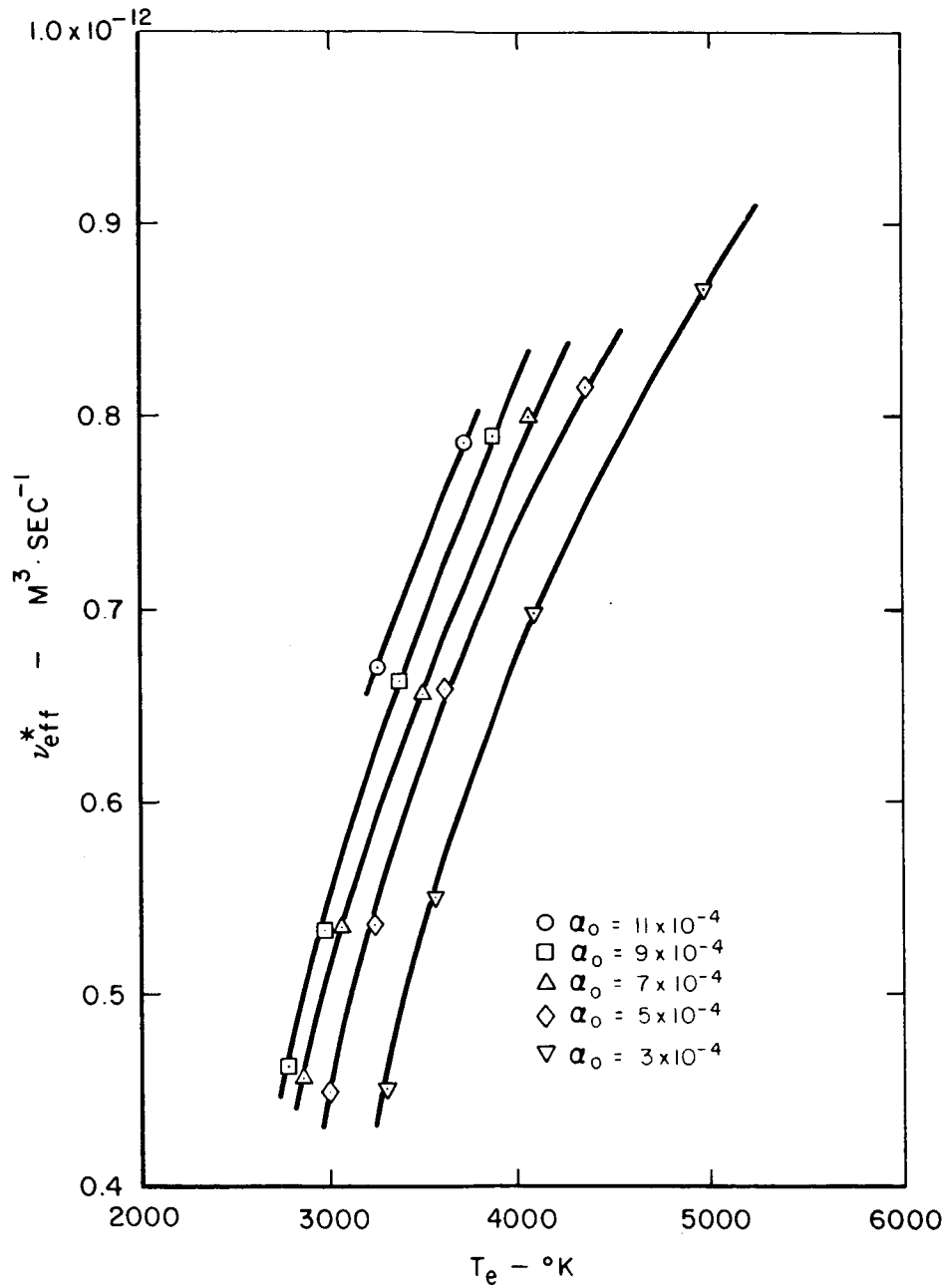
VARIATION OF DEGREE OF IONIZATION
WITH DISCHARGE CURRENT AND PRESSURE

TEST 6*-j RUNS 1-48

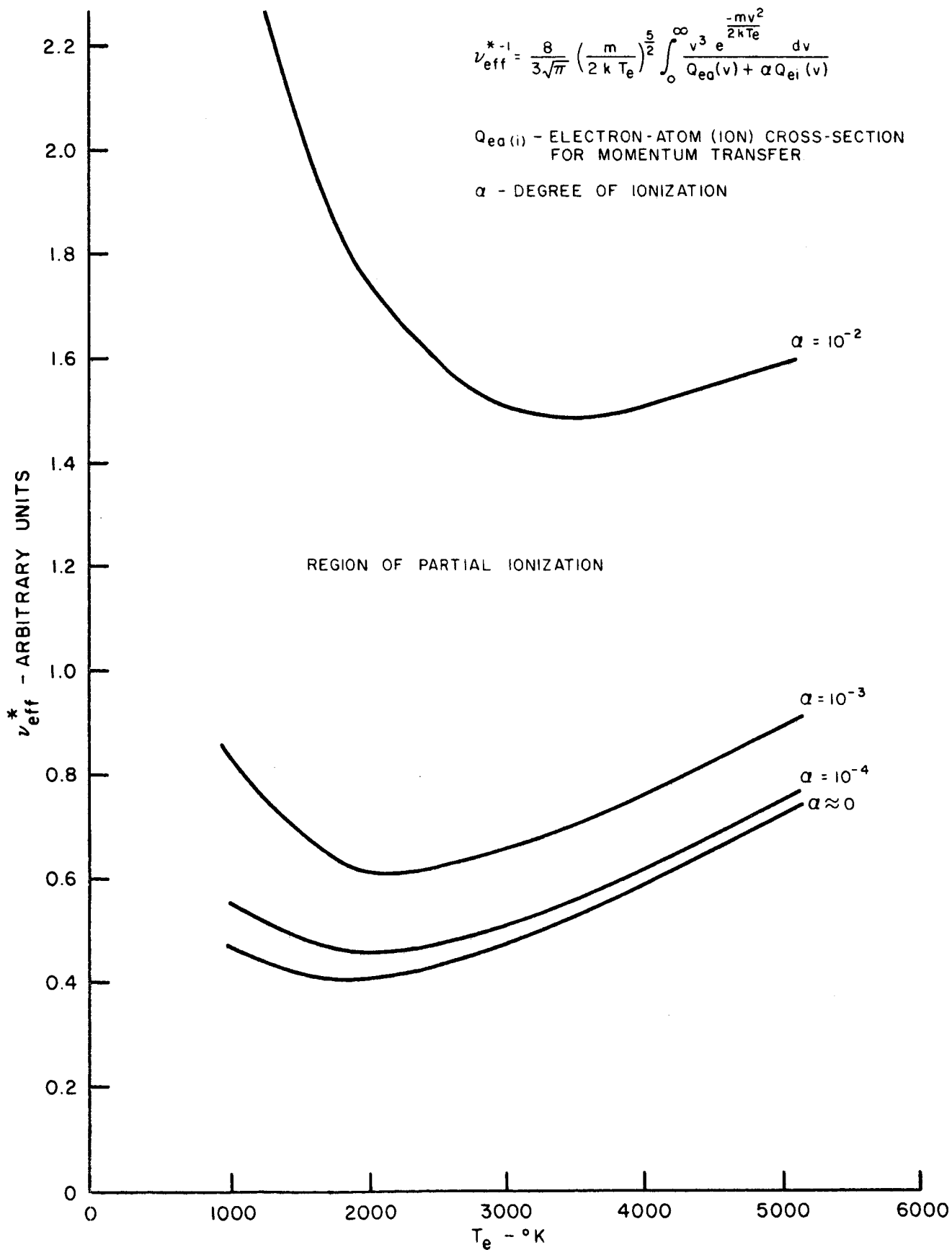


NORMALIZED EFFECTIVE COLLISION FREQUENCY VARIATION
WITH DEGREE OF IONIZATION AND ELECTRON TEMPERATURE

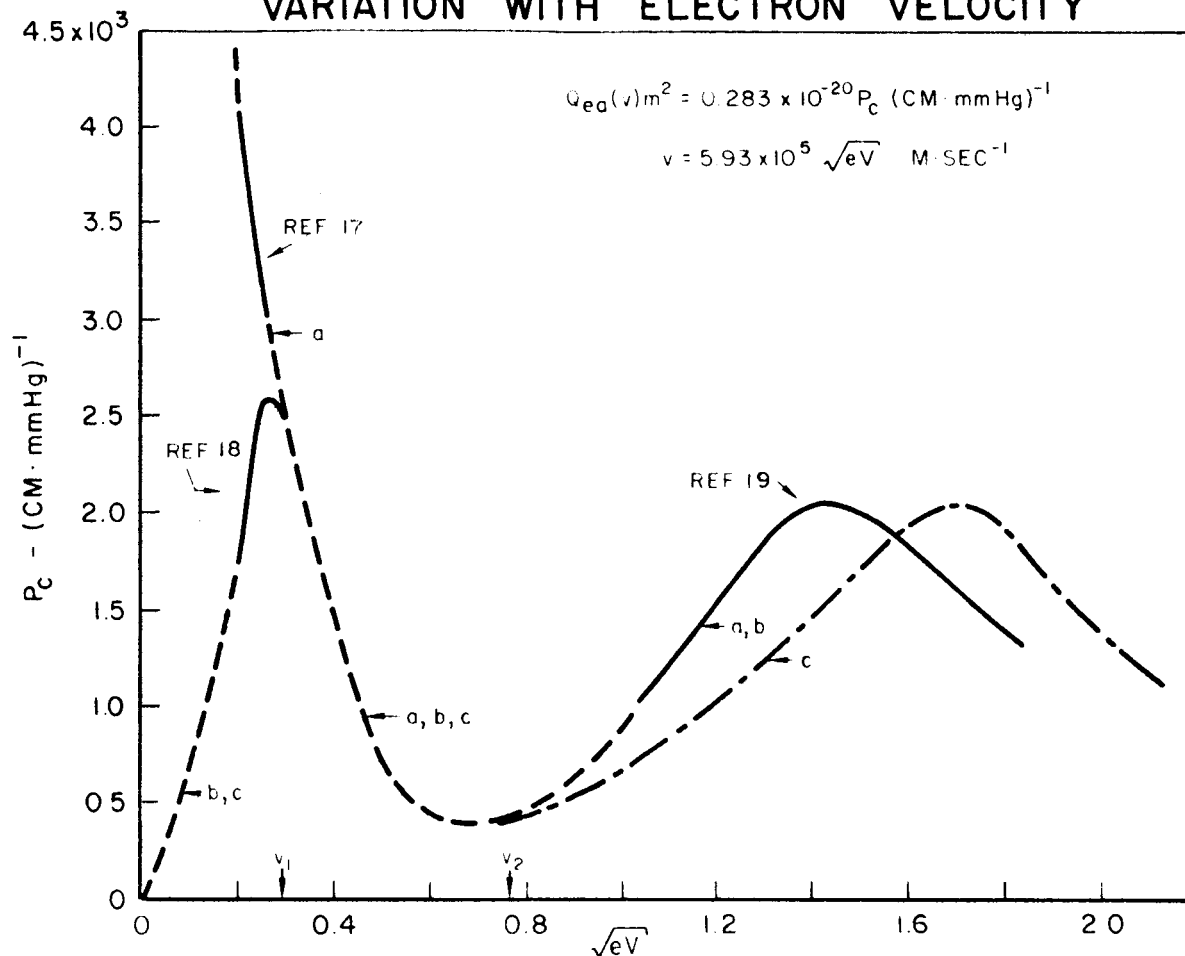
TEST 6*-j RUNS 1-48



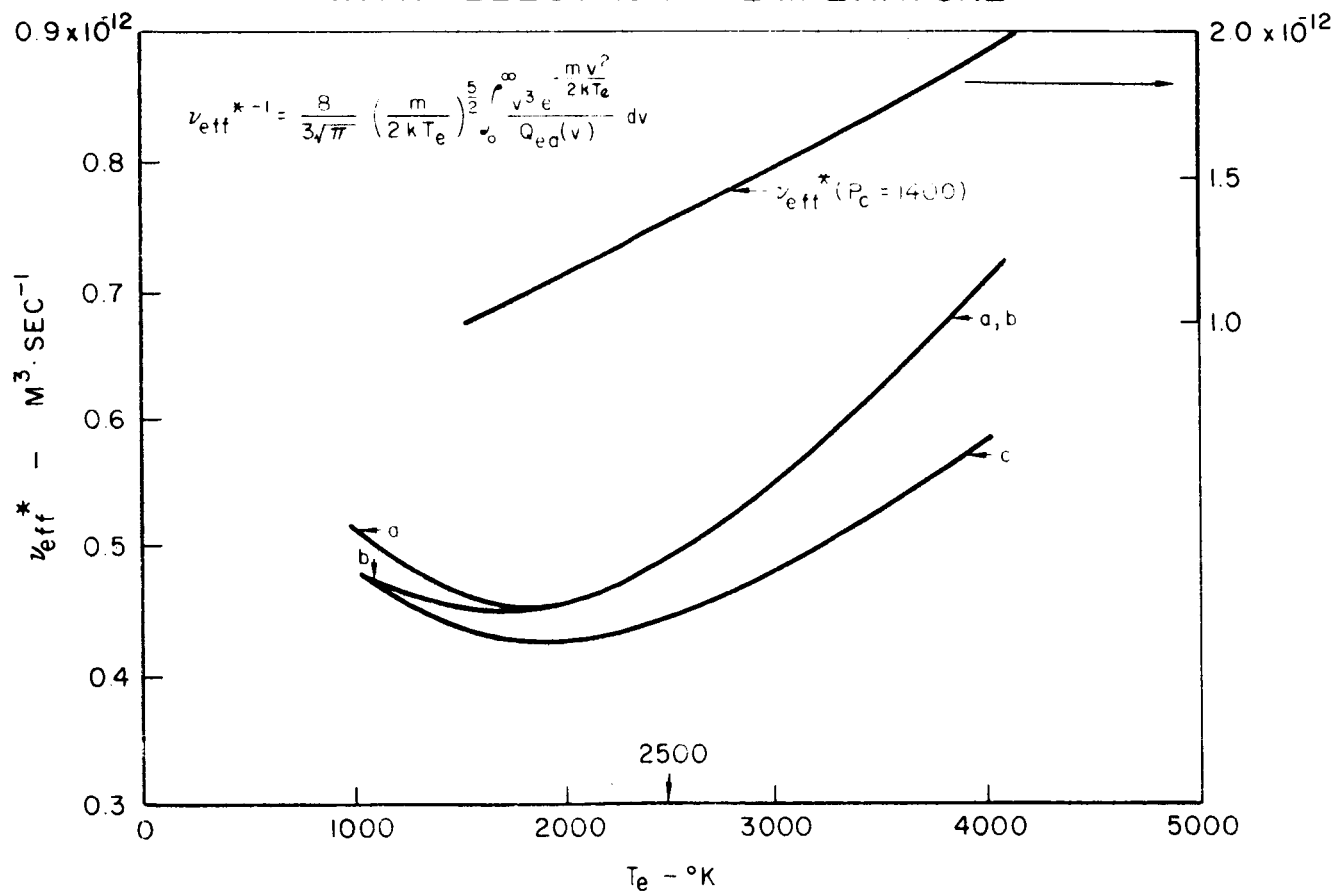
EFFECTIVE ELECTRON CESIUM HEAVY PARTICLE COLLISION FREQUENCY AS A FUNCTION OF ELECTRON TEMPERATURE AND DEGREE OF IONIZATION



ELECTRON CESIUM ATOM COLLISION PROBABILITY VARIATION WITH ELECTRON VELOCITY



NORMALIZED EFFECTIVE COLLISION FREQUENCY WITH ELECTRON TEMPERATURE



APPENDIX I

THE DETERMINATION OF CESIUM ION MOBILITIES FROM
LOW-ENERGY CESIUM ION-ATOM CROSS SECTIONS.

by R. H. Bullis

United Aircraft Corporation Research Laboratories, East Hartford, Connecticut

Presented at
the
IEEE Thermionic Converter Specialist Conference
Cleveland, Ohio
October 26, 27, and 28, 1964

The Determination of Cesium Ion Mobilities from
Low-Energy Cesium Ion-Atom Cross Sections*

by R. H. Bullis

United Aircraft Corporation Research Laboratories, East Hartford, Connecticut

Abstract

Low-energy cesium ion-atom total collision cross sections have been measured over an energy range of 0.12 to 9.7 eV in a modified Ramsauer cross-section experiment in which significant perturbations, caused by contact potential effects, have been eliminated by employing an electroformed collision chamber. The results of this investigation were initially reported at the Thermionic Conversion Specialist Conference in Gatlinburg, Tennessee, in October 1963.¹ Further analysis of this cross-section information has been made to determine the diffusion cross section of cesium ions in cesium vapor. The calculated diffusion cross section is related to a mobility which is a meaningful parameter in the analysis of loss rates of ions from diffusion dominated plasmas. Also a brief description is presented of the techniques which can be employed to take into account the influence of the velocity of the target cesium atom on the extremely low-energy cross-section information. The calculated atomic cesium ion mobilities are related to other mobility measurements reported in the literature and mobilities determined from extrapolations of high-energy charge exchange cross-section information made by Sheldon.²

Introduction

To obtain a complete understanding of the properties of the neutralization plasma that exists in arc-mode converters, the loss rate of ions from the plasma must be accurately known so that estimates can be made of the production rate of ions required to sustain the enhanced degree of ionization.

The total collision cross section of cesium ions with cesium atoms has been measured in a modified Ramsauer collision cross-section experiment in which contact potential effects have been eliminated from the measurements by the use of an electroformed collision chamber. At energy levels below 1.0 eV, electric fields on the order of millivolts per cm can significantly perturb the trajectory of a cesium ion in a magnetic field giving rise to spurious experimental results. Therefore, the basic concept employed in these total collision cross-section measurements was to create a field-free region in which the energy of the ion beam could be uniquely determined and in which the interaction of the cesium ion beam with neutral cesium atoms could take place. By electroforming the

*Portions of this work were supported by the National Aeronautics and Space Administration under Contract NASr-112 and Contract NAS3-4171.

collision chamber of copper and by controlling the grain size of the copper plate on the inner surface of the chamber, significant perturbations of the trajectory of the ion beam, as it passed through the collision chamber due to contact potential or thermoelectric effects were eliminated. The geometry of the collision chamber as shown schematically in Fig. 1, served to uniquely define the radius of curvature of the ion beam in the magnetic field. Three points of constraint of the ion beam defined by the geometry of the collision chamber are the entrance and exit slits and the constricted portion in the center of the chamber. The energy of the ion beam passing through the chamber was then determined from a knowledge of the magnitude of the applied magnetic field and the radius of curvature determined by the collision chamber geometry. Re-entrant slits were employed on the collision chamber to prevent the penetration into the chamber of perturbing electric fields produced in other parts of the system. A more detailed description of the complete system, as well as the techniques employed to obtain the total collision cross-section information, is presented in Ref. 1. From a knowledge of the measured total collision cross section, which is dependent on the geometry of the collision chamber, it is possible to determine the magnitude of the charge exchange cross section by completely classical techniques. The charge exchange cross section can then be related to the diffusion cross section which is used in the calculation of ion mobilities.

Description of the Measurements

The total collision cross section was determined by measuring the attenuation of the ion beam produced by increases in the neutral cesium pressure in the collision chamber. The ion beam current exiting the collision chamber for a particular chamber pressure and ion beam energy is related to the ion beam current which exits the chamber for essentially zero cesium pressure in the chamber by the following expression:

$$I = I_0 e^{-p_0 P_t x} \quad (I-1)$$

where

I_0 is the ion beam current exiting the chamber for zero cesium pressure in the chamber

I is the ion beam current exiting the chamber for a finite cesium pressure in the chamber

p_0 is the cesium pressure in the collision chamber reduced to 273°K,

P_t is the total collision probability which is the number of collisions per cm of path per mm of pressure

x is the path length of the ion beam in the collision chamber.

In this measurement, P_t is the total collision probability which is composed of resonance charge exchange interactions as well as elastic scattering events. The geometry of the collision chamber was such that any collision event which produced a deflection of the ion beam of greater than 0.0074 radians in the laboratory system was detected. Therefore, to relate this beam data to the effective mobility of a cesium ion, both the minimum deflection angle for detection and the fact that both resonant charge exchange and elastic scattering events were detected in these measurements have to be taken into account in the analysis.

Analysis of the Cross-Section Information

Sheldon³ has shown by classical techniques that it is possible to calculate both the differential as well as the total collision cross section of cesium ions interacting with cesium atoms. A brief outline of the Sheldon analysis is presented herein so that the techniques employed to extract the charge exchange cross-section information from the measured total collision cross section can be clearly understood. Sheldon's thesis (Ref. 3) should be consulted for a more detailed description of the actual classical analysis.

By treating the particle orbit classically and determining the charge exchange probability, P_0 , by the impact parameter method of Demkov,⁴ the differential charge exchange cross section, $\sigma_x(\epsilon, \theta)$, can be determined from the following equation

$$\sigma_x(\epsilon, \theta) = P_0 \sigma(\epsilon, \pi - \theta) \quad (\text{I-2})$$

where

- $\sigma(\epsilon, \theta)$ is the total classical scattering cross section
- θ is the apparent scattering angle in the center of mass coordinate system
- P_0 is the charge exchange probability which is zero for elastic collisions and ranges from zero to one with an average value of approximately 1/2 for charge exchange collisions. Therefore, in this analysis P_0 is either 1/2 or zero.

Then $\sigma_e(\epsilon, \theta)$ which is the actual elastic scattering cross section can be determined from the relation

$$\sigma_e(\epsilon, \theta) = (1 - P_0) \sigma(\epsilon, \theta) \quad (\text{I-3})$$

The total classical scattering cross section is given by

$$\sigma(\epsilon, \theta) = - \frac{b}{\sin \theta} \frac{db}{d\theta} \quad (\text{I-4})$$

where

b is the impact parameter which produces a scattering angle θ in the center of mass system.

The two-particle cesium problem can be generalized to a hypothetical single-particle scattering problem. The conservation of energy and momentum for the one-particle system can be written in polar coordinates in the form

$$E_T = \frac{1}{2} \mu (\dot{r}^2 + r^2 \dot{\phi}^2) + U(r) = \frac{1}{2} \mu u^2 = \text{const.} \quad (\text{I-5})$$

and

$$\mathcal{L} = \mu r \dot{\phi} = \mu u b = \text{const.} \quad (\text{I-6})$$

where

r and ϕ are polar coordinates of the particle.

These equations combine to give the following equation of motion

$$\frac{dr}{d\phi} = \frac{r^2}{b} \sqrt{1 - \frac{b^2}{r^2} - 2 \frac{U(r)}{\epsilon}} \quad (\text{I-7})$$

where $\epsilon = \frac{1}{2} \mu u^2$

For the case of cesium, the potential function, $U(r)$, has the form suggested by Margenau⁵

$$U(r) = - \frac{V}{r^4} \quad (\text{I-8})$$

where

$$V = \frac{e^2 \alpha}{2} \quad (\text{I-9})$$

and

α is the polarizability of Cs, and
 e is the electronic charge.

The classical scattering cross section due to a polarization potential, which can be obtained from this formulation has the form

$$\sigma(\epsilon, \theta) \sin \theta = \sqrt{\frac{2V}{\epsilon}} \frac{1}{4} \frac{(1-k^2)^2 (1+k^2)^{\frac{1}{2}}}{k^3 [(1-k^2)K(k) + (1+k^2)B(k)]} \quad (\text{I-10})$$

where

$K(k), B(k)$ are complete elliptic integrals of the first kind

$$K = r_1/r_0$$

and r_1, r_0 are roots of the equation

$$r^2 \sqrt{1 - \frac{b^2}{r^2} - 2 \frac{U(r)}{\epsilon}} = 0 \quad (\text{I-11})$$

The angular dependence is introduced in the form

$$\theta = 2 \sqrt{1+k^2} K(k) - \pi \quad (\text{I-12})$$

Eq. (I-10) then becomes generalized in the form of

$$\sigma(\epsilon, \theta) \sin \theta \approx \frac{1}{8\theta^{\frac{3}{2}}} \sqrt{\frac{6\pi V}{\epsilon}} \quad (\text{I-13})$$

which is the classical differential scattering cross section due to a polarization potential. This cross section can then be used to determine the differential charge exchange cross section $\sigma_x(\epsilon, \theta) \sin \theta$ and the differential elastic scattering cross section $\sigma_e(\epsilon, \theta) \sin \theta$. Being able to predict the differential elastic

scattering cross section, as it will be shown later, is the key to the analysis used to determine the charge exchange cross section from the measured total collision cross sections. From Eqs. (I-2) and (I-3) and a knowledge of the classical differential scattering cross section, it is possible to calculate the actual differential elastic scattering cross section and the differential charge exchange cross section, as shown typically in Fig. 2. The total scattering cross section, which includes elastic as well as charge exchange events, corresponds to the total area under this curve. To determine the differential elastic scattering portion of this curve, the value of the polarizability, α , must be known to determine the differential charge exchange cross section. The critical angle for cutoff that corresponds to the largest impact parameter for which charge exchange can occur must be known. This critical angle which is energy dependent can be determined from a knowledge of the energy dependence of the high-energy charge exchange cross-section data.

In the actual measurement of the total collision cross section, the minimum scattering angle that can be detected by the system must be taken into account in the interpretation of the cross-section information. Sheldon has denoted this angle as θ_M . For a completely classical analysis of the data to be valid, the resolution of the system must be such that $\theta_M > \theta^*$ where θ^* , according to Massey and Mohr,⁶ can be approximated by

$$\theta^* \approx \frac{\lambda}{2r_0} = \frac{\pi \hbar}{\mu v r_0} \quad (\text{I-14})$$

where

λ is the deBroglie wavelength of the colliding particles

$\mu = m_1 m_2 / m_1 + m_2$ the reduced mass

v is the initial relative velocity

r_0 is the characteristic molecular dimension

For systems with resolutions below the critical angle, θ^* , the uncertainty in the position of the particle is greater than the resolution of the system, and therefore, the cross-section information cannot be interpreted on an entirely classical basis.

For cesium ion-atom cross-section measurements, this critical angle for interaction energies of 0.12 eV is slightly less than the resolution of the system employed in the measurements. The significance of the minimum resolution of the system can be vividly evaluated by referring to Fig. 2, in which the differential elastic scattering cross section is plotted for an energy of 0.025 eV. As θ_M , the resolution of the system or the minimum detectable scattering angle decreases to zero, the predicted differential cross section on a classical basis approaches infinity. Therefore, the minimum detectable scattering angle, θ_M , must be taken into account very carefully in order to accurately predict the correct magnitude of the total collision cross section detected by experimental measurements. By the same token, the differential charge exchange cross section, which is essentially large-angle scattering, is unaffected by the minimum resolution of the system. The total area under the differential cross-section curve,

shown in Fig. 2, represents the total collision cross section which includes charge exchange interactions. Sheldon has evaluated the magnitude of this area in the following manner

$$\sigma_T(\epsilon, \theta) = 2\pi \int_{\theta_M}^{\pi} \sigma_e(\epsilon, \theta) \sin \theta d\theta + 2\pi \int_{\theta_M}^{\pi-\theta'_C} \sigma_X(\epsilon, \theta) \sin \theta d\theta \quad (I-15)$$

where

θ_M is the angular resolution of the system, and
 θ'_C is the cutoff angle which is the particle scattering angle corresponding to the largest impact parameter for which charge exchange can occur.

If it is required that $\theta_M < \theta'_C$

$$\sigma_T(\epsilon, \theta_M) = 2\pi \int_{\theta_M}^{\pi} \sigma(\epsilon, \theta) \sin \theta d\theta \quad (I-16)$$

then

$$\sigma_T(\epsilon, \theta_M) = \int_0^{b_{MIN}} 2\pi b db = \pi b_M^2 \quad (I-17)$$

which leads to

$$\sigma_T(\epsilon, \theta_M) \approx \pi \sqrt{\frac{3\pi V}{2\epsilon \theta_M}} \quad (I-18)$$

for the condition of θ_M small.

Therefore, the measured total collision cross section can be determined in this manner with the only characteristic atomic parameter required in the prediction being the polarizability, α , if the condition is met that $\theta_M < \theta'_C$. Since θ'_C is dependent on energy, the assumption that $\theta_M < \theta'_C$ holds for the complete energy range of any measurement must be carefully investigated. The error caused in the determination of the total collision cross section can be very significant if this condition is not met.

The expression derived by Sheldon to predict the value of the critical angle of cutoff is given by the following:

$$\theta'_C = \frac{3\pi^3 V}{8\epsilon(A - B \ln \epsilon)^4} \quad (I-19)$$

where

A and B are constants derived on the basis of the behavior of high-energy charge exchange cross-section information.

Using the values of $A = 27.2 \text{ \AA}$ and $B = 1.53 \text{ \AA}$ as derived from the reported high-energy charge exchange information of Marino, et al,⁷ and a value of $\alpha = 52.3 \text{ \AA}^3$ as determined from the very accurate polarizability measurements of Salop, et al,⁸ the critical cutoff angle can be determined. The critical angle for cutoff for total collision cross section measurements in cesium over the energy range of 0.1 to 10 eV ranges from 4×10^{-2} radians at 0.1 eV to 1.4×10^{-3}

radians at 10 eV. Therefore, for the total collision cross-section measurements conducted in this present experiment, the condition that $\theta_M < \theta'_C$ is not met for the entire energy range. In discussions with Sheldon⁹ it was agreed that significant changes in the predicted total collision cross section based on Eq. (I-18) would occur for the condition where $\theta_M > \theta'_C$.

Subsequently, Sheldon⁹ has derived a correction factor to account for this condition which results in a term of the form

$$1 + \frac{1}{2} \left[\sqrt{\frac{\theta_M}{\theta'_C}} - 1 \right] \quad (\text{I-20})$$

This term should be multiplied by the predicted total collision cross-section value of Eq. (I-18) to obtain an estimate of the total area under the curve of Fig. 2, which represents the measured total collision cross section.

A comparison of the experimentally measured cross section with the theoretical results predicted on the basis of this analysis is shown in Fig. 3. The agreement between the predicted and the experimentally measured cross section is better at high energies, as can be seen from this figure. It should be remembered that the magnitude of the predicted total cross section is extremely sensitive to the magnitude of the critical cutoff angle which is predicted theoretically on the basis of the energy dependence of the high-energy charge exchange cross-section information. At low energies polarization effects can become appreciable, and as a result, the critical angle for cutoff, predicted on the basis of the energy dependence of the high-energy charge exchange cross-section information, can be significantly different from the actual critical cutoff angle.

Determination of the Charge Exchange Cross Section

As has been outlined in the previous section, the measured total collision cross section shown in Fig. 3 is comprised of elastic scattering events as well as charge exchange encounters. The resolution of the collision chamber determines the minimum angle of deflection counted in these measurements as a scattering event. As shown in Fig. 2, the differential elastic scattering cross section increases rapidly as the minimum detectable scattering angle decreases. The minimum resolution of the collision chamber used in these studies was 0.0074 radians. Therefore, the contribution of elastic scattering events to the total collision cross section is π times the area under the differential elastic scattering cross-section curve between $\theta = 0.0148$ radians and π radians as shown in the inset of Fig. 2. The elastic scattering cross section can also be represented by the integral

$$\sigma_e(\epsilon, \theta_M) = 2\pi \int_{\theta_M}^{\pi} (1-P_0) \sigma(\epsilon, \theta) \sin \theta d\theta \quad (\text{I-21})$$

Shown in Fig. 4 is the variation with energy in the magnitude of the elastic scattering contribution to the total collision cross section. This value is only a portion of the true total elastic collision cross section. Once again it should be pointed out that the magnitude of the elastic scattering events

contributing to the measured total collision cross section is strongly dependent on the minimum scattering angle which can be detected by the geometry of the collision chamber. The total charge exchange cross section can be determined by subtracting from the measured total collision cross section the contribution due to elastic scattering events. The charge exchange cross section, which is predominantly large angle scattering, is not subject to corrections due to the finite resolution of the system. In order to extract the charge exchange information from the measured total collision cross-section information, the polarizability of cesium as measured by Salop, et al,⁸ is the only atomic parameter which must be known. Shown in Fig. 5 is the value of the charge exchange cross section determined by this technique.

The energy dependence of the charge exchange cross section has a form which can be approximated by

$$\sigma_x = \frac{A}{\sqrt[3]{E}} \quad (I-22)$$

where

A is a constant with a value of $2300 \text{ \AA}^2 \text{ ev}^{1/3}$.

Mobility Determination

By using the semiclassical version of the quantal theory presented by Holstein and Dalgarno,¹⁰ it can be shown that the diffusion cross section of an ion moving in its parent gas is twice the cross section for the resonance charge transfer process. This result has also been derived by Sheldon.³ Shown in Fig. 6 is the variation of the diffusion cross section with energy. It is this cross section which should be used to determine the mobility of a cesium ion. In the case of arc-mode thermionic converters, the effective mobility of the atomic ions existing in the plasma can be determined by integrating the measured diffusion cross section over the ion energy distribution. As outlined by Sheldon,¹¹ the mobility, μ , can be determined by

$$\mu = \frac{3\sqrt{\pi}}{8} \frac{e}{\sqrt{mKT}} \frac{1}{N\bar{Q}} \quad (I-23)$$

where

m is the ion or atom mass and

$$\bar{Q} = \frac{1}{2(KT)^3} \int_0^\infty \epsilon^2 \sigma_D e^{-\epsilon/KT} d\epsilon \quad (I-24)$$

The value of the ion mobility determined from these measurements is $0.011 \text{ cm}^2/\text{Vsec}$. The expression used to calculate the mobility in the low-field limit was derived by Holstein.¹² The low-field limit requires that the energy gain of the particles between collisions be small in comparison to their mean thermal energy. For the case of the converter, electrostatic probe measurements, Ref. 13, indicate that field strengths in the emitter sheath range from 300 - 1500 volts per meter. The typical ion mean free path is on the order of 10^{-4} cm for a converter operating at a pressure of 1 mm. The energy gain per collision for this condition is

obviously extremely small in comparison to the mean thermal energy of the ions or gas atoms in the interelectrode space. Therefore, the low-field approximation should definitely be valid under these conditions.

Corrections for the Target Gas Velocity

At ion beam energies of 0.12 eV, the energy of the target gas atoms in the collision chamber becomes appreciable in comparison to the ion beam energy. Under these conditions an analysis presented by Russek¹⁴ must be used to correct the cross-section information for the velocity of the target gas atoms. The corrected cross section can be expressed in the following terms

$$\sigma(T, \theta) = \int_0^\infty f(v_t) dv_t \int_0^\pi \frac{1}{2} \sin \alpha d\alpha \int_0^{2\pi} \frac{1}{2\pi} d\phi \left[\frac{\sin \Theta}{\sin \theta} J \left(\begin{matrix} \Theta, \phi \\ \theta, \phi \end{matrix} \right) \sigma_c^\Theta \right] \quad (I-25)$$

where

$f(v_t)$ is the distribution function of the velocities of the target gas atoms

α is the angle between the target and the projectile velocity in the laboratory frame

σ_c^Θ is the cross section in the center of mass frame

$J \left(\begin{matrix} \Theta, \phi \\ \theta, \phi \end{matrix} \right)$ is the Jacobian transformation from the center of mass to laboratory coordinate system

Russek¹⁵ has found that solutions to Eq. (I-25) are valid as long as the velocity of the target gas atom is not equal to or greater than the velocity of the projectile. For the case of a distribution of target gas velocities, the solutions will be valid until a significant portion of the target atoms has velocities equal to or greater than the projectile velocity. Numerical techniques have to be resorted to in order to obtain a solution for the case where the target particles have a Maxwellian distribution as in the case of the present cross-section measurements.

Conclusions

The cesium ion mobility can be determined from total collision cross-section measurements by employing completely classical techniques to ascertain the percentage of the measured total collision cross section which is due to charge exchange collisions. The charge exchange cross section determined from the low-energy total collision cross-section measurements has been found to be higher than extrapolations of high-energy charge exchange cross sections presented by Sheldon.¹¹ A comparison between the extrapolated and the predicted charge exchange cross sections based on low-energy total collision cross-section measurements is presented in Fig. 7. Since there is almost an order of magnitude variation in the extrapolated values of the charge exchange cross section at low energies, the validity of these cross-section values is subject to question. At energies below

1.0 eV polarization effects, which are extremely difficult to include in the extrapolations of high-energy data, can appreciably increase the charge exchange cross section. Therefore, due to polarization effects the charge exchange cross sections determined from low-energy total collision cross-section measurements could easily be expected to be higher than values predicted on the basis of high-energy extrapolations, even though attempts have been made to include in these extrapolations polarization effects. As a result of the fact that the charge exchange cross section determined on the basis of these total collision cross-section measurements is higher than the extrapolated values, the mobility determined from these measurements is lower than the mobilities calculated from the extrapolated high-energy charge exchange information. A comparison can be made of the calculated value of mobility determined from these measurements of $0.011 \text{ cm}^2/\text{Vsec}$ with the mobility values determined by Sheldon from extrapolations of high-energy charge exchange cross sections which are presented in Fig. 8. Of secondary importance in the comparison of the various predicted mobilities is the form of the approximation of the diffusion cross section used in the evaluation of the average diffusion cross section (Eq. I-24). The approximation of diffusion cross section by the form $A / \sqrt[3]{\epsilon}$, which was used predominately because of the ease in handling the integral, tends to weight the low-energy contribution to the cross-section value more heavily than the type of approximation used by Sheldon in Ref. 11.

To accurately estimate the cesium ion mobility applicable to converter conditions, the effective mobility, which is essentially energy dependent, must be determined by integrating the diffusion cross section over the ion energy distribution.

Acknowledgements

The author would like to acknowledge the many helpful discussions that he has had with Dr. H. Williamson of the Research Laboratories of United Aircraft Corporation in the course of the preparation of this paper.

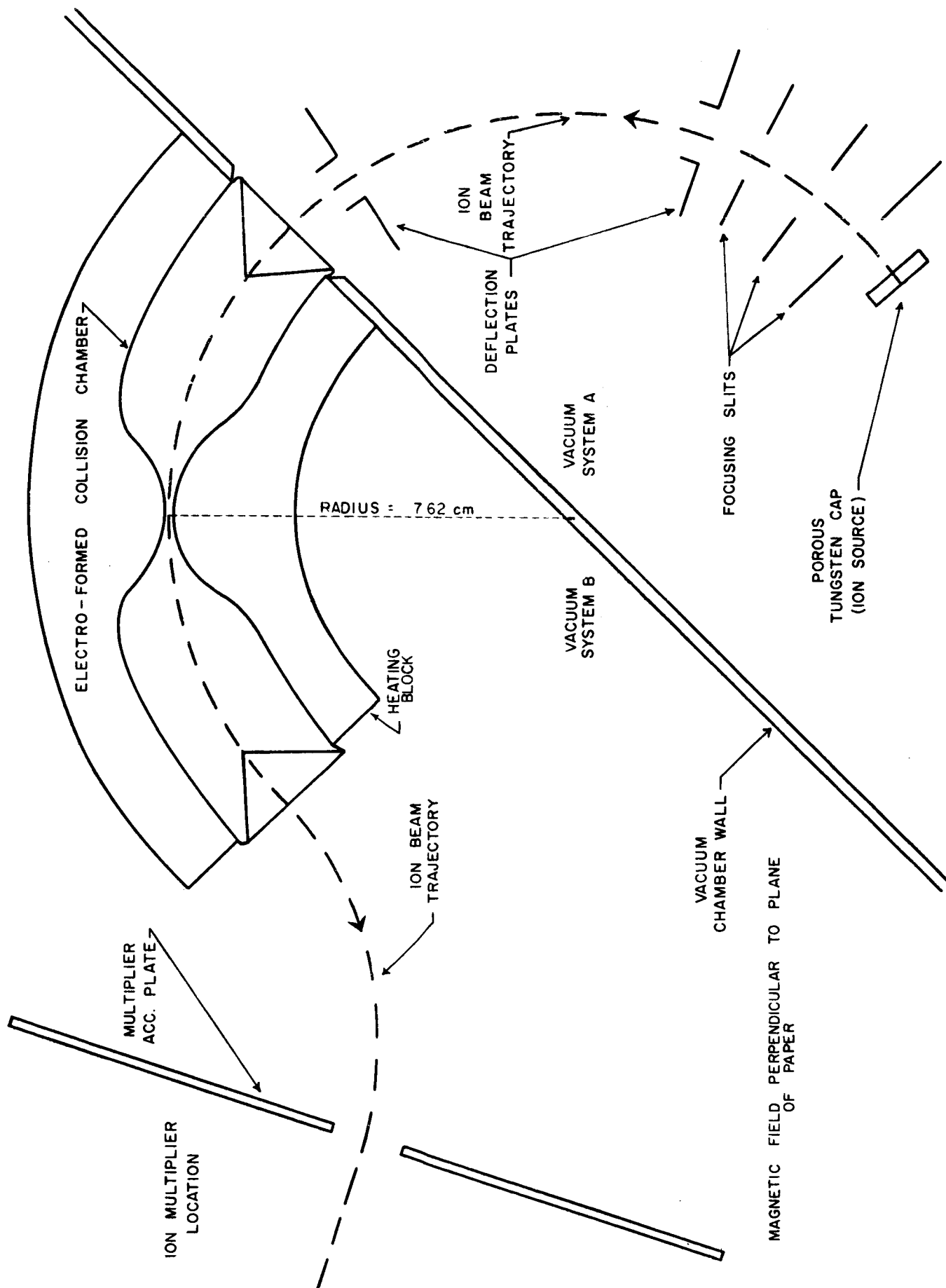
REFERENCES

1. R. H. Bullis, "Low Energy Cesium Ion-Atom Collision Cross Sections," IEEE Thermionic Conversion Specialist Conference Proceedings, October 7, 8, and 9, 1963, Gatlinburg, Tennessee.
2. J. W. Sheldon, "Mobility of Positive Ions in Their Own Gas: Determination of Average Momentum-Transfer Cross Section," NASA Technical Note D-2408, August 1964.
3. J. W. Sheldon, "Semiclassical Calculation of the Differential Scattering Cross Section with Charge Exchange: Cesium Ions in Cesium Vapor," Ph.D. Thesis for Agricultural and Mechanical College of Texas, January 1964.
4. Yu. N. Demkov, Ann. Leningr. Univ. 146, 74 (1952).
5. H. Margenau, Phil. of Sci. 8, 603 (1941).
6. H. S. W. Massey and C. B. O. Mohr, Atomic and Molecular Processes (edited by D. R. Bates, Academic Press, New York, 1962), Chap. 17.
7. L. L. Marino, A. C. H. Smith, and E. Caplinger, Phys. Rev. 128, 2243 (1962).
8. A. Salop, E. Pollack, and B. Bederson, Phys. Rev. 124, 1431 (1961).
9. J. W. Sheldon, Personal communication.
10. T. Holstein and A. Dalgarno, Atomic and Molecular Processes (edited by D. R. Bates, Academic Press, New York, 1962), Chap. 17.
11. J. W. Sheldon, Journ. App. Phys. 34, 2 (1963).
12. T. Holstein, J. Phys. Chem 56, 832 (1952).
13. R. H. Bullis and W. J. Wiegand, "Characteristics of the Neutralization Plasma in the Arc-Mode Thermionic Converter," presented at the IEEE Thermionic Specialist Conference, Cleveland, Ohio, October 26, 27, and 28, 1964.
14. A. Russek, Phys. Rev. 120, 5 (1960).
15. A. Russek, Personal communication.
16. R. M. Kushnir, B. M. Palyukh, and L. A. Sena, Bulletin of the Academy of Sciences, USSR Physical Series 23, 995 (1959).

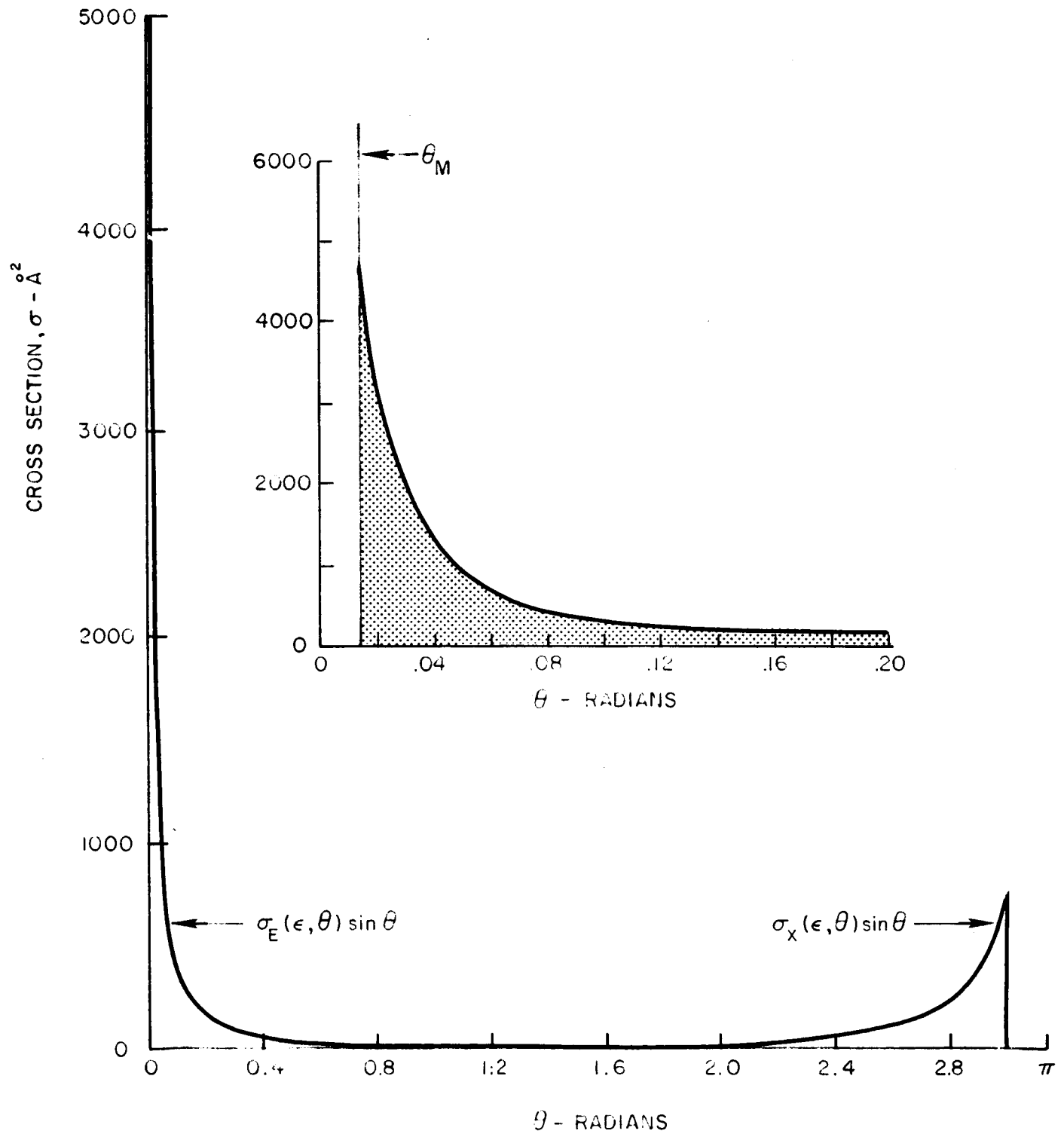
References (Continued)

17. A. M. Bukhteev and Yu. F. Bydin, Bulletin of the USSR Academy of Sciences Physical Series, Transactions of the First All-Union Conference on Electron and Ionic Collisions 24, 966 (1960).
18. R. M. Kushnir and I. M. Buchma, Bulletin of the USSR Academy of Sciences Physical Series, Transactions of the First All-Union Conference on Electron and Ionic Collisions 24, 8 (1960).
19. R. C. Speiser and R. H. Vernon, "Cesium Ion-Atom Charge Exchange Scattering," ARS Space Flight Report to the Nation, October 9 - 15, 1961, New York City.

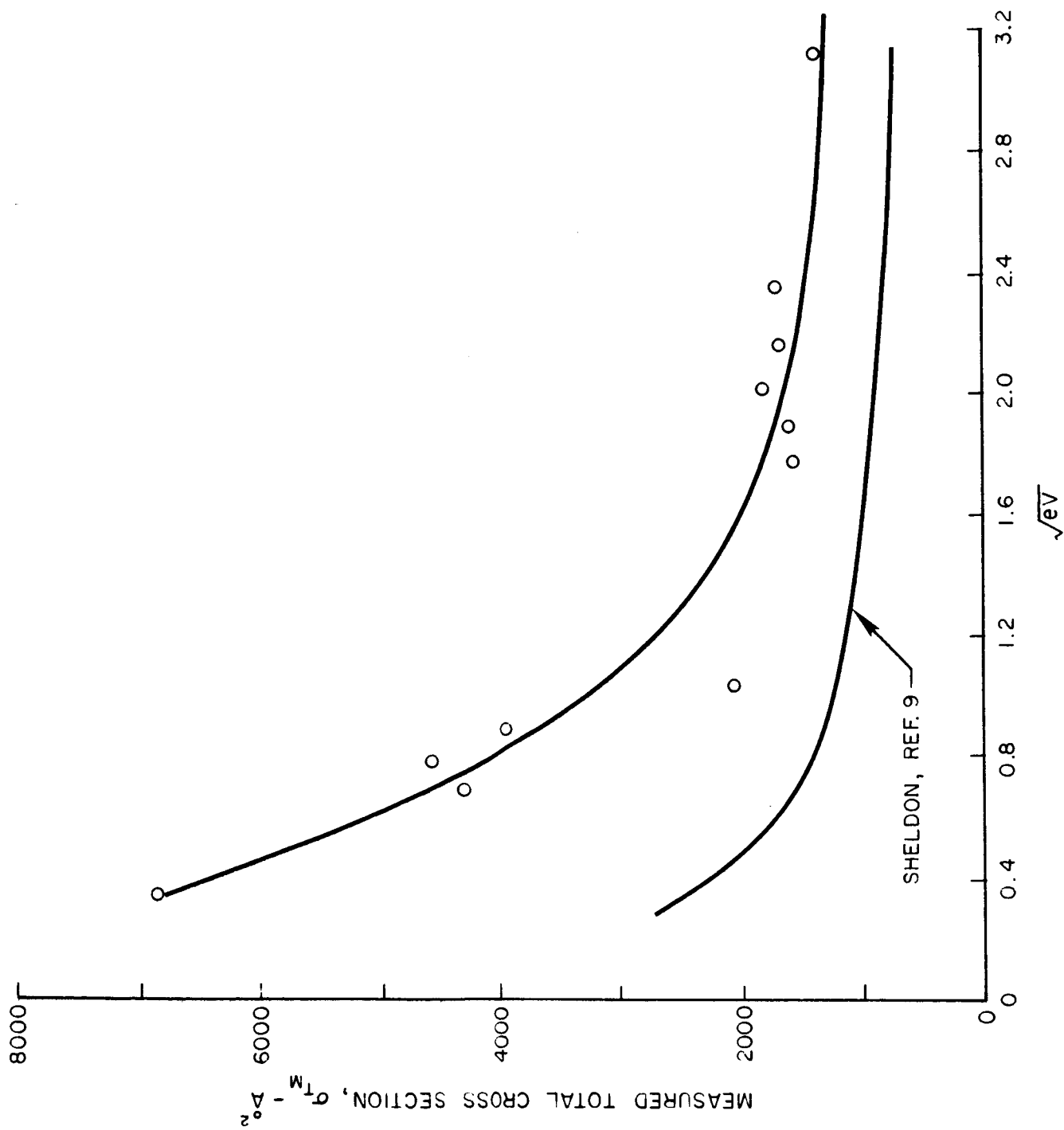
SCHEMATIC DIAGRAM OF ION COLLISION CROSS-SECTION APPARATUS



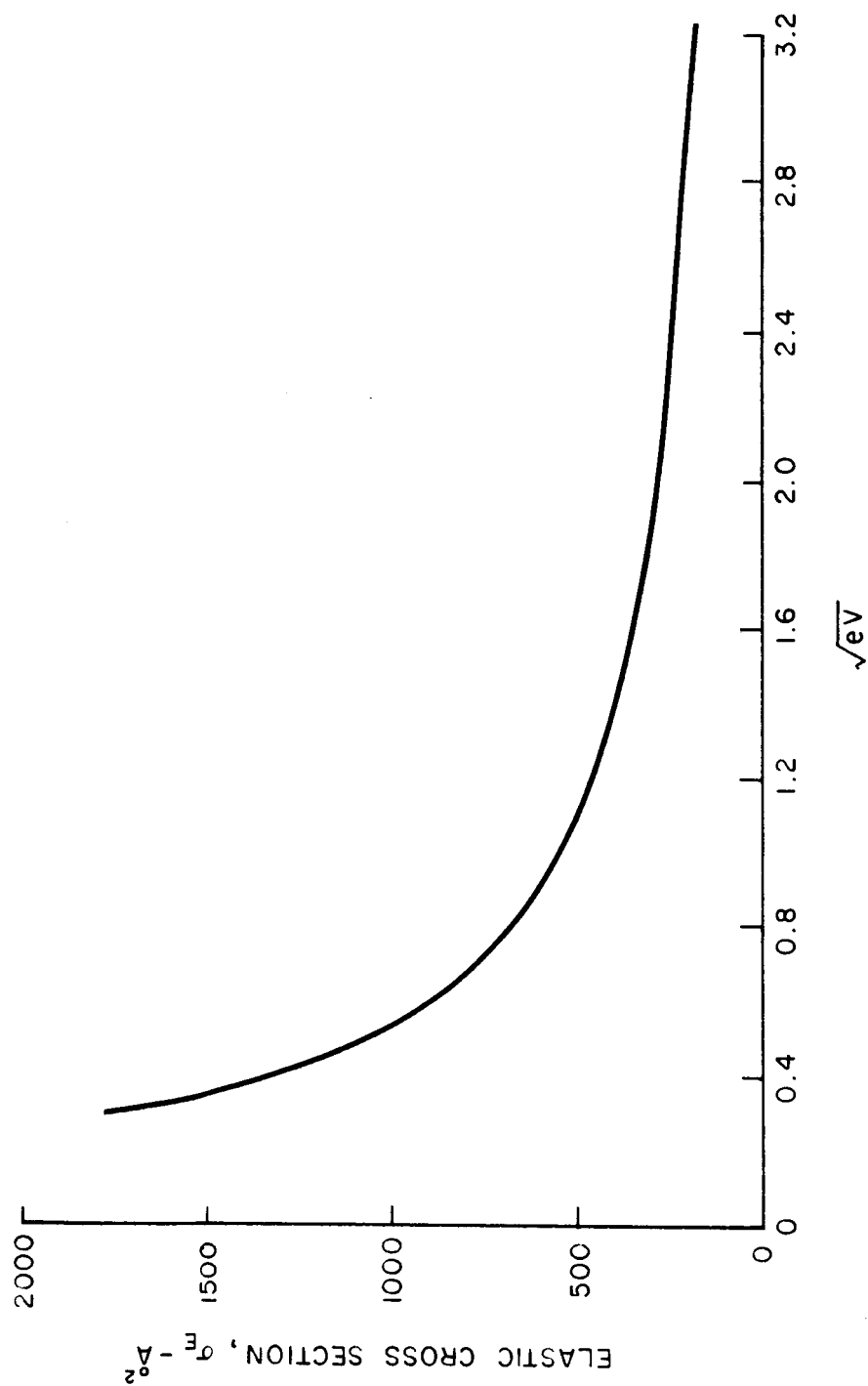
DIFFERENTIAL CROSS SECTION



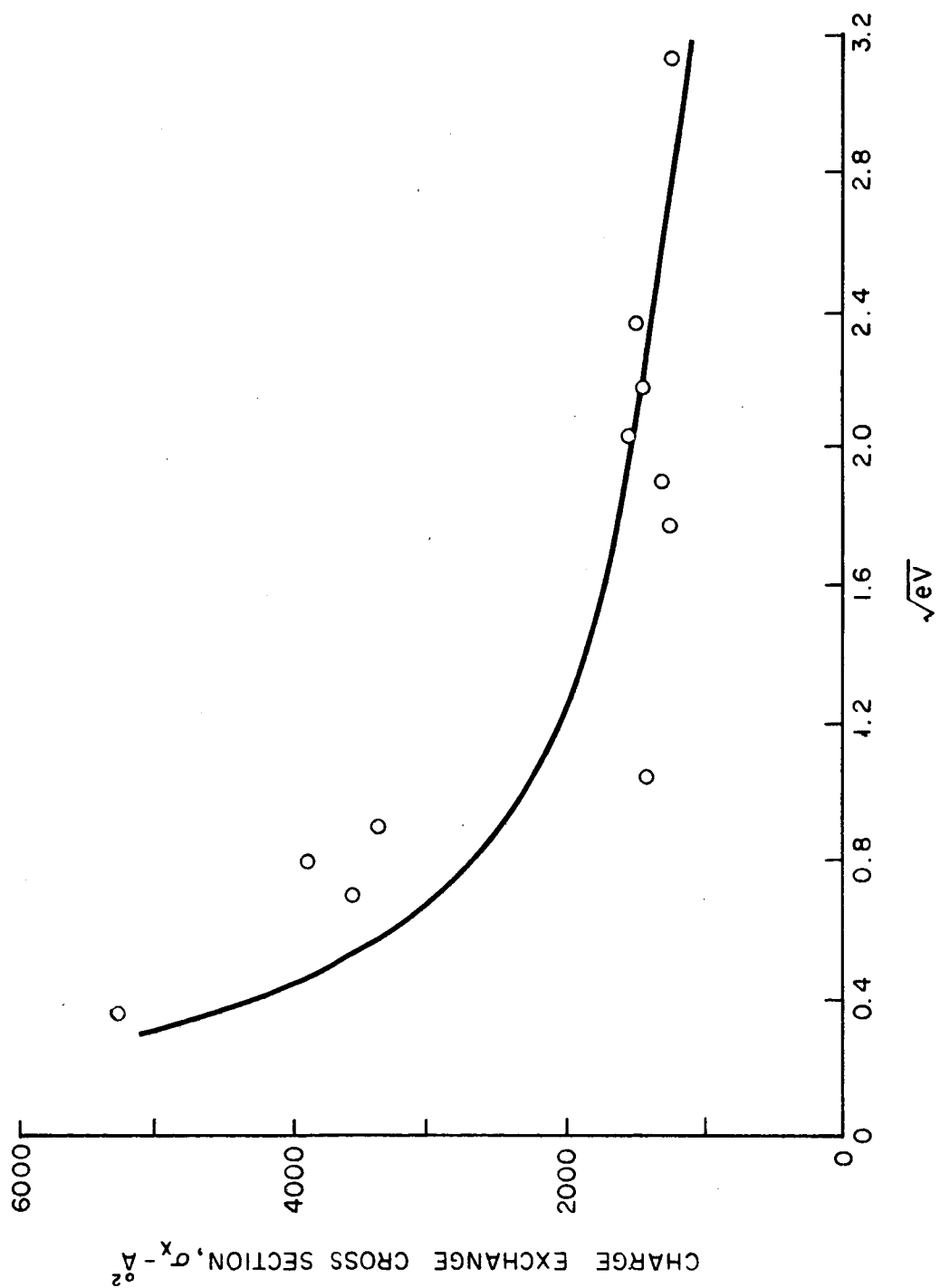
MEASURED TOTAL COLLISION CROSS SECTION



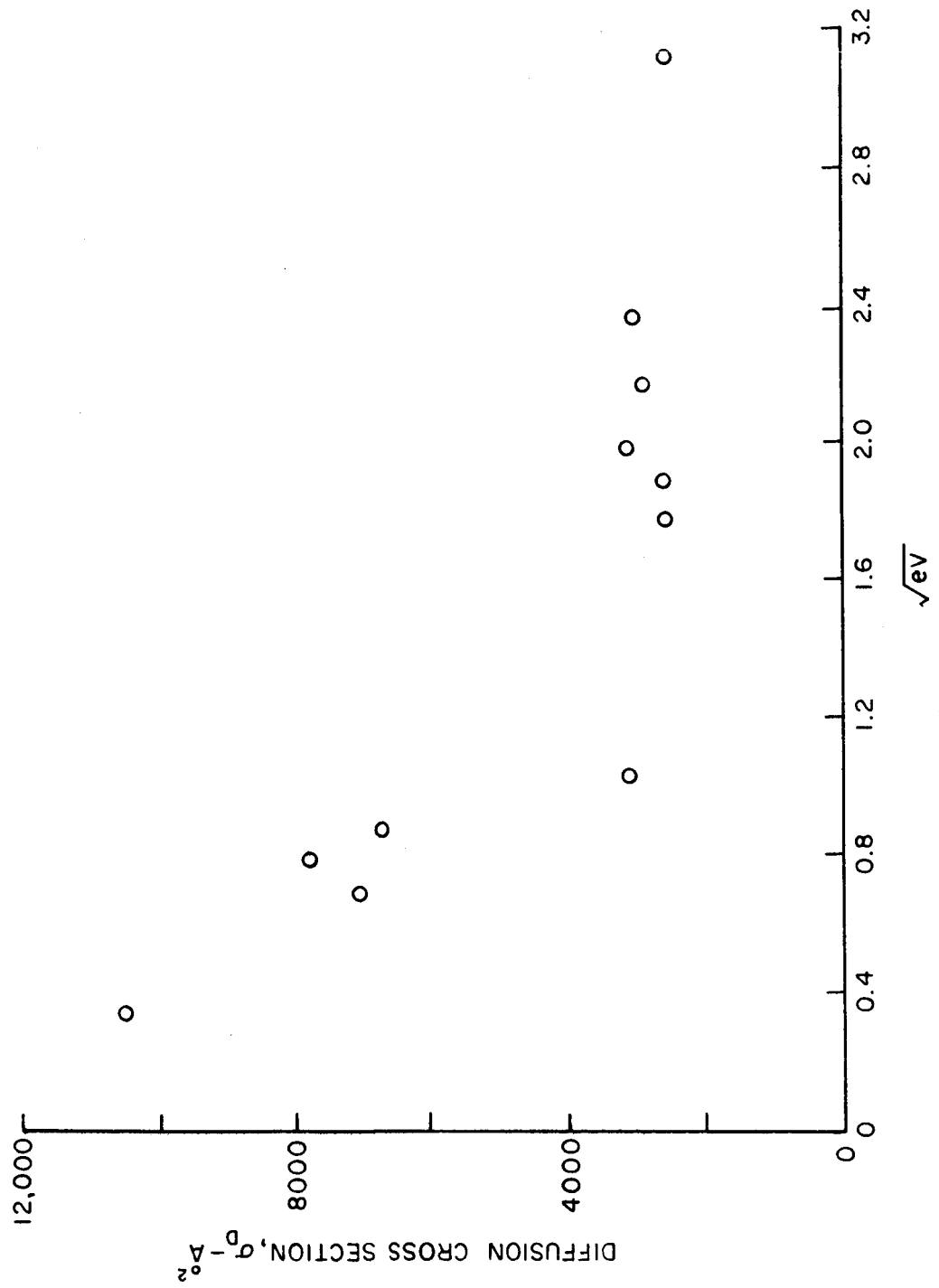
CALCULATED ELASTIC CROSS SECTION



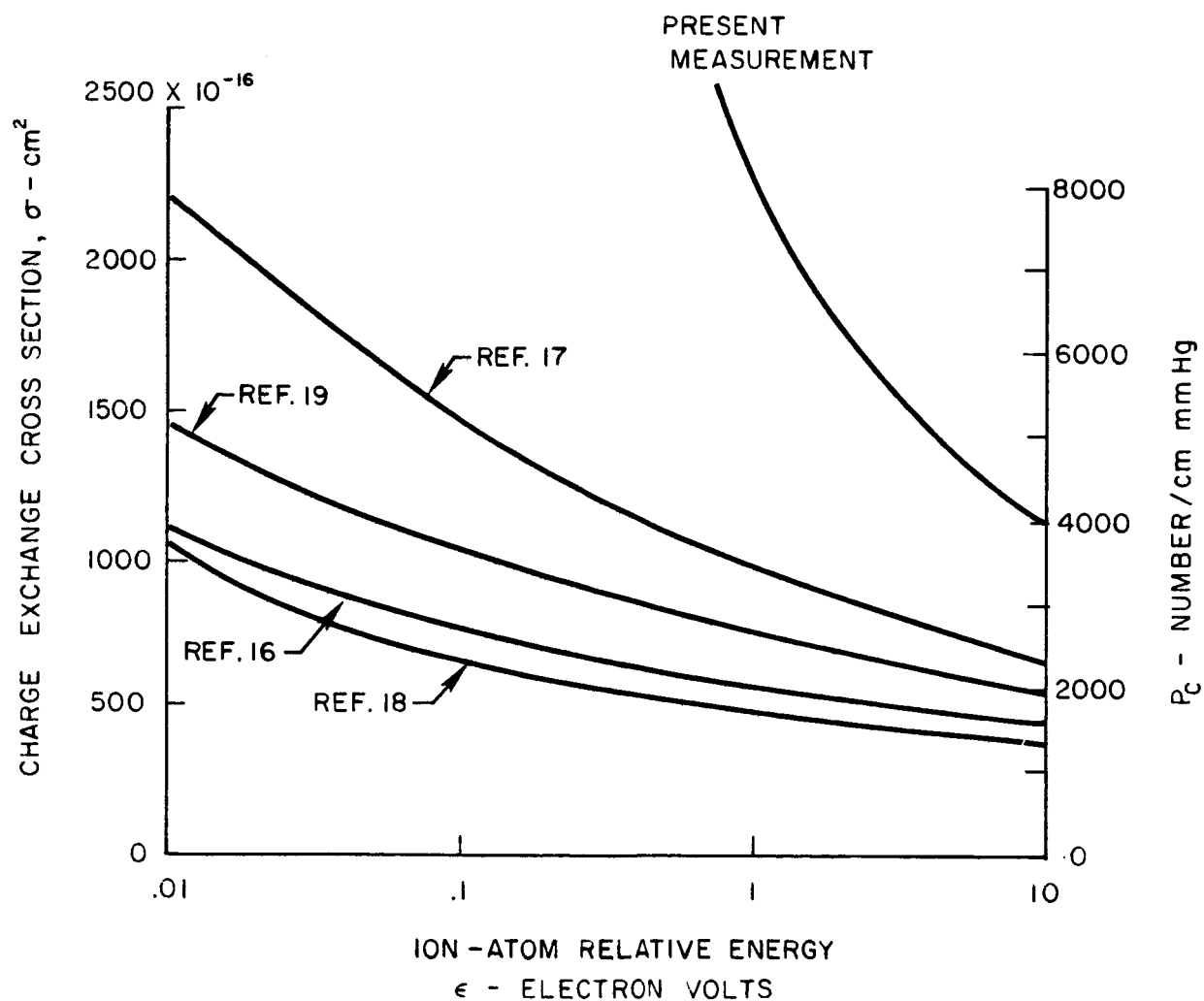
CALCULATED CHARGE EXCHANGE CROSS SECTION



CALCULATED DIFFUSION CROSS SECTION



EXTRAPOLATED CHARGE EXCHANGE CROSS SECTIONS



CALCULATED MOBILITIES

CONSTANT	CONSTANT	ION MOBILITY		
A	B	μ		
\AA	$\text{\AA}/\ln \text{ eV}$	sq cm / V-sec		
		NEW CALC.	PREVIOUSLY REPORTED	REF.
23.97	1.50	$0.0784 \pm .0034$	0.0736	16
22.52	1.15	$0.0914 \pm .0016$	0.0880	18
31.62	3.12	$0.0401 \pm .0003$	0.0361	17
27.40	1.84	$0.0603 \pm .0015$	0.0552	19

APPENDIX II

AVERAGING PROCESS TO ACCOUNT FOR RADIAL ELECTRON DENSITY VARIATIONS

In order to properly average the current density over the cross section of the positive column, the radial variation in electron density must be taken into account. From Eq. 6 the current flow through the positive column can be written

$$I = \frac{n_e e^2}{m \nu_{eff}} E \cdot A \quad \text{II-1}$$

where A is the cross section of the discharge tube. For a radial electron density variation, Eq. II-1 becomes

$$I = 2\pi \frac{e^2 E}{m \nu_{eff}} \int_0^R n_e(r) r dr \quad \text{II-2}$$

where integration in the circumferential direction has been carried out. For $n_e(r)$ approximated by a parabolic distribution, as is nearly the case (Fig. 7), Eq. II-2 becomes

$$I = 2\pi \frac{e^2 E}{m \nu_{eff}} \int_0^R n_{eo} \left(1 - \frac{r^2}{R^2}\right) r dr \quad \text{II-3}$$

$$I = \frac{n_{eo} e^2}{m \nu_{eff}} E \cdot \frac{\pi R^2}{2} \quad \text{II-4}$$

It is apparent from Eq. II-4 that the effective collision frequency determination would be in error by a factor of two in this case if the electron density was not averaged over the cross section. When a Bessel function is used in place of a parabolic distribution the indicated error would be approximately a factor of 2.5. For the determination of effective collision frequency in this report (Fig. 11), a parabolic distribution was assumed.

DISTRIBUTION LIST FOR UNITED AIRCRAFT CORPORATION

Contract No. NAS3-4171
Semiannual and Final Reports

	<u>No. of Copies</u>
Aerojet General Nucleonics San Ramon, California Attention: K. Johnson	1
Aerospace Corporation El Segundo, California Attention: Librarian	1
Air Force Cambridge Research Center (CRZAP) L. G. Hanscom Field Bedford, Massachusetts	1
Air Force Spacial Weapons Center Kirtland Air Force Base Albuquerque, New Mexico Attention: Chief, Nuclear Power Division	1
Air Force Systems Command Aeronautical Systems Division Flight Accessories Laboratory Wright-Patterson AFB, Ohio Attention: ASRMFP-2/E, A. E. Wallis	1
Allison Division General Motors Corporation Indianapolis 6, Indiana Attention: Don L. Dresser	1
Aracon Laboratories Virginia Road Concord, Massachusetts Attention: S. Ruby	1
Argonne National Laboratory 9700 South Cass Avenue Argonne, Illinois Attention: Aaron J. Ulrich	1

C-920243-6

Illinois Institute of Technology
Research Institute
10 West 35th Street
Chicago 16, Illinois
Attention: D. W. Levinson

1

Atomics International
P.O. Box 309
Canoga Park, California
Attention: Robert C. Allen
Charles K. Smith

1

1

The Babcock & Wilcox Company
1201 Kemper Street
Lynchburg, Virginia
Attention: Russel M. Ball

1

Battelle Memorial Institute
505 King Avenue
Columbus 1, Ohio
Attention: David Dingee
Don Keller

1

1

The Bendix Corporation
Research Laboratories Division
Northwestern Highway
Detroit 35, Michigan
Attention: W. M. Spurgeon

1

Bureau of Ships
Department of The Navy
Washington 25, D.C.
Attention: B.B. Rosenbaum
John Huth

1

1

Consolidated Controls Corporation
Bethel, Connecticut
Attention: David Mends

1

Mr. John McNeil
Market Development Manager
Research Division
Allis-Chalmers Manufacturing Company
Post Office Box 512
Milwaukee, Wisconsin

1

; C-920243-6

Douglas Aircraft Company
Missile & Space Engineering
Nuclear Research (AZ-260)
3000 Ocean Park
Santa Monica, California
Attention: A. Del Grosso

1

Electro-Optical Systems, Incorporated
300 North Halstead Avenue
Pasadena, California
Attention: A. Jensen

1

Ford Instrument Company
32-36 47th Avenue
Long Island City, New York
Attention: M. Silverberg

1

General Atomic
P.O. Box 608
San Diego 12, California
Attention: R. W. Pidd
L. Yang
A. Weinberg

1

1

1

General Electric Company
Missile & Space Vehicle Department
3198 Chestnut Street
Philadelphia 4, Pennsylvania
Attention: Library

1

General Electric Company
Knolls Atomic Power Laboratory
Schenectady, New York
Attention: R. Ehrlich

1

General Electric Company
Power Tube Division
One River Road
Schenectady 5, New York
Attention: D. L. Schaefer

1

General Electric Company
Nuclear Materials & Propulsion Operation
P.O. Box 15132
Cincinnati 15, Ohio
Attention: J. A. McGurty

1

C-920243-6

General Electric Company
Research Laboratory
Schenectady, New York
Attention: Volney C. Wilson
John Houston

1
1

General Electric Company
Special Purpose Nuclear System Operations
Vallecitos Atomic Laboratory
P.O. Box 846
Pleasanton, California
Attention: E. Blue
B. Voorhees

1
1

General Motors Corporation
Research Laboratories
Warren, Michigan
Attention: F. E. Jamerson

1

Hughes Research Laboratories
3011 Malibu Canyon Road
Malibu, California
Attention: R. C. Knechtli

1

Institute for Defense Analyses
1666 Connecticut Avenue, N.W.
Washington 9, D.C.
Attention: R. C. Hamilton

1

Jet Propulsion Laboratory
California Institute of Technology
4800 Oak Grove Drive
Pasadena, California
Attention: Arvin Smith
Peter Rouklove

1
1

Los Alamos Scientific Laboratory
P.O. Box 1663
Los Alamos, New Mexico
Attention: G. M. Grover
Walter Reichelt

1
1

Marquardt Corporation
Astro Division
16555 Saticoy Street
Van Nuys, California
Attention: A. N. Thomas

1

C-920243-6

National Aeronautics & Space Administration
Scientific & Technical Information Facility
P. O. Box 5700
Bethesda 14, Maryland
Attention: NASA Representative

2 copies and 1 repro.

National Aeronautics & Space Administration
Goddard Space Flight Center
Greenbelt, Maryland
Attention: Joseph Epstein

1

National Bureau of Standards
Washington, D.C.
Attention: Library

1

Oak Ridge National Laboratory
Oak Ridge, Tennessee
Attention: Library

1

Office of Naval Research
Power Branch
Department of the Navy
Washington 25, D.C.
Attention: Cdr. J.J. Connelly, Jr.

1

Power Information Center
University of Pennsylvania
Moore School Building
200 South 33rd Street
Philadelphia 4, Pennsylvania

1

Pratt & Whitney Aircraft Corporation
East Hartford 8, Connecticut
Attention: William Lueckel
Franz Harter

1

1

Radio Corporation of America
Electron Tube Division
Lancaster, Pennsylvania
Attention: Fred Block

1

Radio Corporation of America
David Sarnoff Research Center
Princeton, New Jersey
Attention: Karl G. Hernqvist
Paul Rappaport

1

1

C-920243-6

Martin - Nuclear
Division of Martin-Marietta Corporation
P.O. Box 5042
Middle River 3, Maryland
Attention: J. Levedahl 1

Massachusetts Institute of Technology
Cambridge, Massachusetts
Attention: Wayne B. Nottingham 1
E. N. Carabateas 1

National Aeronautics & Space Administration
Western Operations Office
150 Pico Boulevard
Santa Monica, California
Attention: Fred Glaski 1

National Aeronautics & Space Administration
Manned Spacecraft Center
Houston, Texas
Attention: J. D. Murrell 1

National Aeronautics & Space Administration
600 Independence Avenue, N.W.
Washington 25, D.C.
Attention: Fred Schulman 1
James J. Lynch 1
H. Harrison 1
Walter Scott 1

National Aeronautics & Space Administration
Lewis Research Center
21000 Brookpark Road
Cleveland, Ohio 44135
Attention: Roland Breitwieser (C&EC) 1
Robert Migra (NRD) 1
Bernard Lubarsky (SPSD) 1
James J. Ward (SPSD) 1
Herman Schwartz (SPSD) 1
C. Walker (SPSPS) 1
R. Mather (SPSD) 1
H. E. Nastelin (SPSD) 3
John J. Weber (TUO) 1

National Aeronautics & Space Administration
Marshall Space Flight Center
Huntsville, Alabama
Attention: Library 1

C-920243-6
 The Rand Corporation
 1700 Main Street
 Santa Monica, California
 Attention: Librarian 1

Republic Aviation Corporation
 Farmingdale, Long Island, New York
 Attention: Alfred Schock 1

Space Technology Laboratories
 Los Angeles 45, California
 Attention: Kenneth K. Tang 1

Texas Instruments, Incorporated
 P.O. Box 5474
 Dallas, Texas
 Attention: R. A. Chapman 1

Thermo Electron Engineering Corporation
 85 First Avenue
 Waltham 54, Massachusetts
 Attention: George Hatsopoulos 1
 Ned Rasor 1

Thompson Ramo Wooldridge, Incorporated
 7209 Platt Avenue
 Cleveland, Ohio
 Attention: W. J. Leovic 1

United Nuclear Corporation
 Five New Street
 White Plains, New York
 Attention: Al Strasser 1

U.S. Army Signal R & D Laboratory
 Fort Monmouth, New Jersey
 Attention: Emil Kittil 1

U.S. Atomic Energy Commission
 Division of Reactor Development
 Washington 25, D.C.
 Attention: Direct Conversion Branch 1

U.S. Atomic Energy Commission
 Technical Reports Library
 Washington 25, D.C.
 Attention: J. M. O'Leary 3

C-920243-6

U.S. Atomic Energy Commission
Department of Technical Information Extension
P.O. Box 62
Oak Ridge, Tennessee

3

U.S. Atomic Energy Commission
San Francisco Operations Office
2111 Bancroft Way
Berkeley 4, California
Attention: Reactor Division

1

U.S. Naval Research Laboratory
Washington 25, D.C.
Attention: George Haas
Library

1

1

Defense Research Corporation
P.O. Box 3587
Santa Barbara, California
Attention: Harold W. Lewis

1

Westinghouse Electric Corporation
Research Laboratories
Pittsburgh, Pennsylvania
Attention: R. J. Zollweg

1

The Boeing Company
Seattle, Washington
Attention: Howard L. Steele

1

Varian Associates
611 Hansen Way
Palo Alto, California
Attention: Ira Weissman

1